BLANKET ENGINEERING

KEYWORDS: *uncertainty in tritium production, fusion integral experiments, neutronics R&D*

NUCLEAR ANALYSIS OF INTEGRAL EXPERIMENTS ON A Li_2O TEST ASSEMBLY WITH LOCAL HETEROGENEITIES UTILIZING A 14-MeV NEUTRON SOURCE

M. Z. YOUSSEF, A. KUMAR, M. A. ABDOU, and Y. WATANABE
University of California, Los Angeles, School of Engineering and Applied Science
Mechanical, Aerospace, and Nuclear Engineering Department
Los Angeles, California 90095

M. NAKAGAWA, K. KOSAKO, T. MORI, Y. OYAMA, C. KONNO, Y. IKEDA, H. MAEKAWA, and T. NAKAMURA
Japan Atomic Energy Research Institute, Department of Reactor Engineering
Tokai Research Establishment, Tokai-mura, Naka-gun, Ibaraki-ken 319-11, Japan

Received January 20, 1994
Accepted for Publication July 20, 1994

The integral experiments and postanalyses performed in Phase IIC of the U.S. Department of Energy (U.S. DOE)/Japan Atomic Energy Research Institute (JAERI) collaborative program on fusion neutronics focused on test blankets that include the actual heterogeneities found in several blanket designs. In one arrangement, multilayers of Li_2O and beryllium were placed in an edge-on, horizontally alternating configuration, and in the second arrangement, vertical water coolant channels were deployed. The main objective has been to examine the accuracy of predicting key parameters such as tritium production rate (TPR), in-system spectrum, and other reaction rates around these heterogeneities and to experimentally verify the enhancement in TPR by beryllium in the first experiment. The prediction accuracy was examined in terms of calculated-to-experimental values $(c/e)_i$ of the neutronics parameters at several spatial locations. Average local $(c/e)_i$ values were statistically calculated for TPR from Li-6 (T_6) and from Li-7 (T_7) in addition to quantifying the prediction uncertainties in the line-integrated TPR. A relationship was developed between the prediction uncertainty in the integrated TPR and the corresponding values in the total breeding zone. This relationship enabled us to identify which subzone contributes the most to the prediction uncertainty in the overall integrated TPR.

I. INTRODUCTION

Conceptual blanket design for fusion reactors includes heterogeneous arrangement of more than one material that serves a particular function for efficient energy extraction. In solid breeder blankets, the existence of coolant and purge gas channels leads to considerable distortion in the neutron energy spectrum around these heterogeneities. The materials themselves deployed in the blanket have different neutronics characteristics and hence they introduce local, and in some cases, sharp variation in the neutron spectrum at the interfaces of these materials. Often, designers follow homogenization procedure in their calculational models, particularly when the blanket includes complex features of multicomponents, in order to simplify the models used to predict the unclear performance of the blanket. This naturally leads to large uncertainties in the prediction of local effects. Two fusion-oriented integral experiments that focused on these heterogeneities' effects were performed at the Fusion Neutronics Source (FNS) facility at the Japan Atomic Energy Research Institute (JAERI). Unlike the earlier Phase I experiments,[1-3] in Phase IIA, IIB (Refs. 4 through 12), and IIC (the subject of this paper), the incident neutron spectrum on the test assembly closely simulates the incident neutron spectrum in fusion reactors due to the careful selection of materials and configuration. In phase III (Refs. 13 through 18), an annular test assembly totally surrounds a simulated line source. In all

these experiments, the prediction accuracies of key neutronics parameters, such as tritium production rate (TPR) from Li_6 (T_6) and Li_7 (T_7), are checked against the measured ones to arrive at estimates for the uncertainties associated with these parameters. The TPR (both locally and inside zones) is the prime focus in these phases. The prediction accuracy for other parameters (e.g., local and integrated neutron spectrum, several activation reaction rates) were also examined.

In the present work, the prediction uncertainties in TPR (and other parameters) around heterogeneities are examined and expressed in terms of the calculated-to-experimental value, $(c/e)_i$, at the various locations. Estimates to the average uncertainty in local values were made by applying a statistical approach. Since blanket designers are interested in quantifying the prediction uncertainty in the integrated TPR, which has direct relevance to the tritium breeding ratio (TBR), a more rigorous treatment was followed in which the uncertainties in local TPR are propagated to give an estimate of the prediction uncertainties in the line-integrated TPR. The integration is defined to be along the central axis of the test assembly. Additionally, since heterogeneities could, in some cases, divide the breeder zone into several subzones, the prediction uncertainty in each subzone was also estimated and related to the overall uncertainty in the system.

In Sec. II, the experiments performed on heterogeneities' effects are briefly described. More detailed experimental data for these experiments can be found in the companion paper[19] and in Refs. 20 through 23. The calculational methods followed in analyzing these experiments are described in Sec. III. In Sec. IV, we describe the statistical treatment used to derive the prediction uncertainty in local and the line-integrated TPR. The analytical results and comparison to the experimental data are given in Sec. V. The main findings from this study are summarized in Sec. VI.

II. DESCRIPTION OF THE EXPERIMENTS

The test assembly (Li_2O) is placed at one end of a rectangular Li_2CO_3 enclosure of a 20-cm thickness covered by a 5-cm-thick polyethylene (PE) layer to minimize neutron room-return effects. A water-cooled rotating neutron target (RNT) is used to generate the intense 14 MeV neutrons and is located in the inner cavity. The dimensions of the enclosure are shown in Fig. 1 (see Refs. 19 through 21 for details). The two experiments considered are as follows:

1. The water coolant channel (WCC) arrangement: In this experiment the water channels consisted of a 5-mm-thick polyethylene (to simulate water coolant) structured between two layers of stainless steel. One coolant channel was placed behind a 5-mm-thick stainless steel first wall and preceded the Li_2O test assembly (of thickness ~60 cm). Two other coolant channels were placed at a depth of 10 cm, and 20 cm, respectively, from the front surface of the assembly as shown in Fig. 2. A radial drawer was also installed horizontally (see Refs. 20 and 21). The locations and the dimensions of the coolant channels have been chosen to be representative to these channels found in a typical fusion blanket.

2. The multi-layered beryllium edge-on (BEO) arrangement: In this experiment, multilayers of Li_2O and beryllium were arranged in an edge-on, horizontally alternating configuration for a front depth of 30 cm followed by the Li_2O breeding zone (see Figs. 2). Two central drawers and one radial drawer (filled with Li_2O)

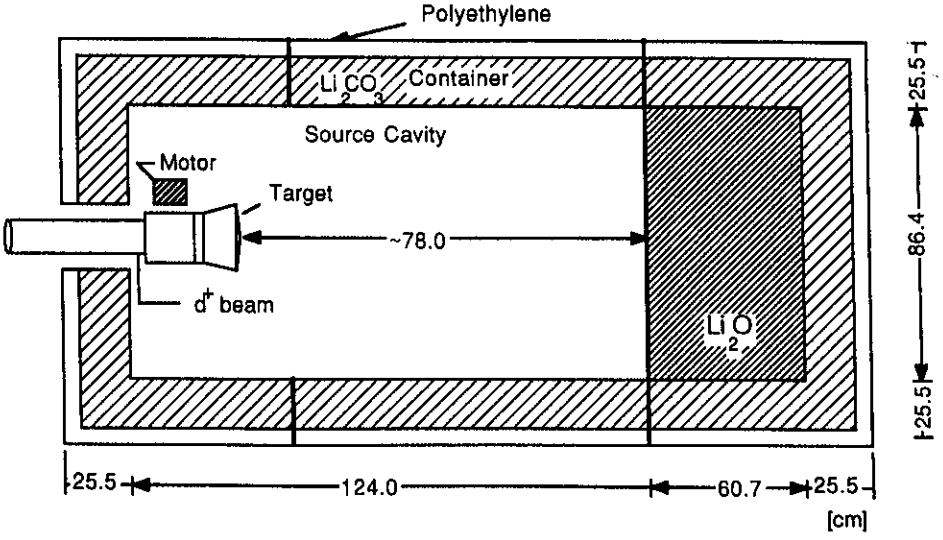

Fig. 1. The test assembly used in Phase IIC experiments.

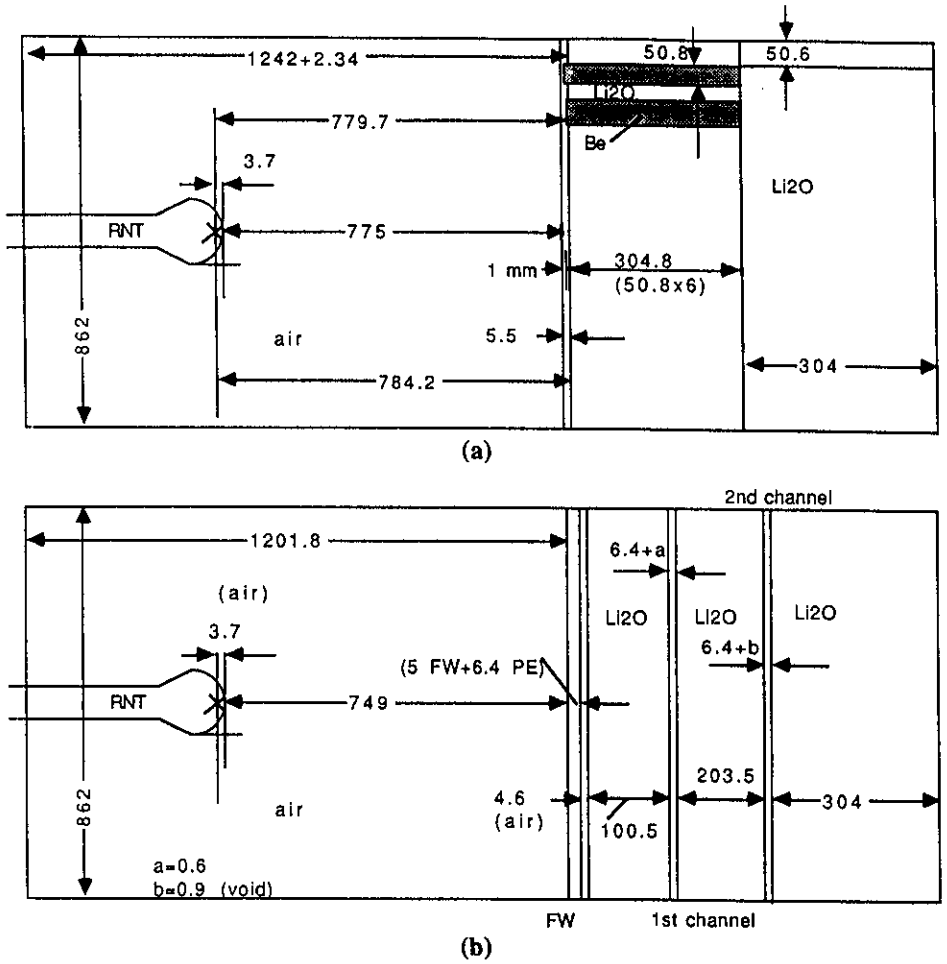

Fig. 2. The inner dimensions (mm) of (a) the BEO and (b) the WCC experiments.

were also installed in this experiment.[20,21] The multilayers arrangement of Be/Li_2O has been chosen after extensive preanalysis aimed at examining the optimal arrangement of equal volumes of beryllium and Li_2O in a front zone of thickness 20 to 30 cm that gives the largest TPR. It was shown that the intermixing of horizontal Be and Li_2O layers in an edge-on arrangement is superior to the vertical arrangement of alternating Be and Li_2O layers as far as the TPR is concerned.[24]

The TPR from Li-6 (T_6) was measured by Li-glass detectors as well as Li-foil detectors. The NE213 detectors were used to measure T_7 by folding the measured spectrum with the response $^7Li(n,n'\alpha)t$ cross section (indirect method). In addition to local TPR measurements, zonal tritium production rates were measured in predesignated blocks along the central drawer (^{7}Li-enriched blocks) and the off-central drawer (^{n}Li-blocks). In-system spectrum measurements were also performed along the central axis using NE213 detectors and proton recoil counters (PRC). Several foil activation measurements of various threshold energies included $^{58}Ni(n,2n)$, $^{115}In(n,n')^{115m}In$, $^{27}Al(n,\alpha)$. Because the $^{197}Au(n,\gamma)$ reaction occurs at all energies, particularly at low neutron energies, this reaction was used to infer the degree of accuracy in predicting T_6. The accuracy of predicting these reactions as well as in-system spectrum can be found in Refs. 19, 20, and 23.

III. CALCULATIONAL METHODS

In analyzing the WCC experiment, both deterministic and Monte Carlo methods were independently used by the U.S. and JAERI. Monte Carlo codes were used in analyzing the BEO experiment. The MCNP (Version 3B) (Ref. 25) was used by the U.S. Department of Energy (U.S.) group along with its pointwise continuous energy/angle cross-section library RMCCS/BMCCS, based on the ENDF/B-V, version-2, data. The MORSE-DD (Ref. 26) code has been used by JAERI, and it utilizes the double differential cross-section library DDL/J3P1 (125 neutron group) based

on the JENDL3/PR1 data file. The codes used by the United States in the two-dimensional Sn method are DOT 5.1 in conjunction with the first collision code, RUFF (Ref. 27). It was necessary to use the RUFF code since it is compatible with DOT 5.1 when the variable mesh feature is used as it is the case in the U.S. calculations. The DOT 5.1 is an advanced version of the DOT 4.3 code.[28] In the JAERI's calculations, the DOT 3.5 (Ref. 29) and GRTUNCL (Ref. 29) codes were used. In these two-dimensional calculations the RUFF and GRTUNCL codes were necessary to use in order to mitigate the ray effect associated with the discrete ordinates methods when applied with an external point source. The P_5-S_{16} approximation was adopted in the U.S. calculations along with the MATXS6D library [80-g, ENDF/B-V (version 2)] which was previously generated using the TRANSX-CTR processing code.[30] The FSXJP7 library (P_7, 125-g) was used in JAERI's calculations with DOT3.5/GRTUNCL codes and is based on JENDL3/PR2. In folding the NE213 experimental data to obtain measured values for T_7, the JENDL3/PR2 data for the $^7Li(n,n'\alpha)t$ cross section was used. (Note: the differences between JENDL3/PR1 and JENDL3/PR2 data are as follows: ^7Li: J3PR2 elastic and total cross sections are lower than those in J3PR1 by ~4%. The $^7Li(n,n'\alpha)t$ cross section is the same; the ^6Li: J3PR2 (n,2n) cross section and secondary emission spectrum for inelastic cross section are lower than those in J3PR1 by ~20%.)

The dimensions adopted in the calculations for the two experiments are shown in Fig. 2 (shown are the inner dimensions of the cavity and the test assembly). It was necessary to calculate the angular and energy distribution of the incident neutrons using the Monte Carlo method to account for the complex nature of the rotating neutron target. These calculations were previously discussed.[2,3] The calculational procedures and modeling are very similar to those used in previous phases.[4,6,8,10,11,19-23] The atomic densities of materials used in the WCC and the BEO experiments are given in Table I.

IV. THE PREDICTION UNCERTAINTY IN LOCAL AND INTEGRATED TPR

In quantifying the mean value of the prediction uncertainty in local TPR, we follow the methodology cited

TABLE I

Atomic Densities ($\times 10^{-24}$) of Materials Used in the Two-Dimensional Calculational Model for the Coolant Channel Experiment*

Element	Inner Li_2O (Drawer)	Outer Li_2O	S.S. Between Inner and Outer Li_2O	FW	S.S. Coolant Channel
Fe	4.894−4[a]	1.092−3	2.514−2	6.022−2	5.987−2
Cr	1.358−4	3.027−4	6.976−3	1.683−2	1.514−2
Ni	5.937−5	1.325−4	3.050−3	7.426−3	8.389−3
Mn	1.086−5	2.422−5	5.577−4	8.440−4	9.945−4
			Li_2CO_3		
^6Li	4.250−3	4.215−3	1.719−3		
^7Li	5.314−2	5.270−2	2.425−2		
^{16}O	2.869−2	2.846−2	4.021−2		
	Concrete	Mortar			
H	7.976−3	3.768−2	5.631−4		
Na	7.859−4	5.080−4	8.928−4		
Ca	2.564−3	3.714−3	8.194−5		
Mg	3.824−4	4.687−4			
Si	1.481−2	1.135−2	8.186−5	7.632−4	3.432−4
Al	2.637−3	1.941−3			
K	5.288−4	3.343−4	8.193−4		
C	5.288−4	7.430−4	1.424−2	1.983−4	4.513−5
^{16}O	4.315−2	9.425−3			
Fe	5.859−4	6.810−4			

*PE (coolant channel) H: 8.257−2, C: 4.128−2. PE (outer layer) H: 8.146−2, C: 4.073−2.
[a]Read as 4.894×10^{-4}.

in Ref. 31. At each measuring location, i, an associated $(c/e)_i$ value was obtained. In addition, an experimental error (uncertainty) and calculational error are estimated at each i, designed by σ_{ei} and σ_{ci}, respectively. In principle, the calculational error could include uncertainties due to geometrical modeling, assumptions embedded in the transport calculations used, and uncertainties associated with nuclear data. The combined uncertainty (relative variance) in the $(c/e)_i$ value is given by

$$\sigma_i^2 = \sigma_{ei}^2 + \sigma_{ci}^2 \ , \tag{1}$$

assuming that the relative standard deviations σ_{ei} and σ_{ci} are uncorrelated.

According to Ref. 31, the $(c/e)_i$ value of local TPR, designated by χ_{li}, is weighted by a weighting factor, ω_i, and the mean value, $\bar{\chi}_l$, for local TPR is obtained from the expression

$$\bar{\chi}_l = \frac{\sum_{i=1}^{N} \omega_i \chi_{li}}{\sum_{i=1}^{N} \omega_i} \ , \tag{2}$$

and the relative standard deviation, σ_l, which gives the spread around the mean value $\bar{\chi}_l$ is obtained from the expression

$$\sigma_l^2 = \frac{\sum_{i=1}^{N} \omega_i^2 \sigma_i^2}{\left(\sum_{i=1}^{N} \omega_i\right)^2} \ , \tag{3}$$

where N is the number of the measuring locations. When the weighting factors ω_i's are chosen to be inversely proportional to the combined uncertainty σ_i^2 (i.e., $\omega_i = 1/\sigma_i^2$), then, the relative variance, σ_l^2, is obtained from the expression

$$\sigma_l^2 = 1 \Big/ \sum_{i=1}^{N} (1/\sigma_i^2) \ . \tag{4}$$

In this case, the mean value, $\bar{\chi}_l$, is obtained from the expression

$$\bar{\chi}_l = \frac{\sum_{i=1}^{N} \chi_{li}/\sigma_i^2}{\sum_{i=1}^{N} 1/\sigma_i^2} \ . \tag{5}$$

In the present analysis, the prediction uncertainty (%) is quantified in terms of the parameter $\bar{X}_l = (\bar{\chi}_l - 1) \times 100$ where $\bar{\chi}_l$ is given by Eq. (5).

The procedures applied to estimate the uncertainty in the line-integrated TPR are as follows[32]:

1. Using the calculation data set, $\{z_i, c_i, \sigma_{ci}^2\}$, where z_i's are the measuring locations, ci's are the data values at locations z_i's, and σ_{ci}^2's are the variance of the data values at locations z_i's, find the curve that can best fit the data c_i's (using least-square fitting). The fitting curve in z can be described by polynomial (i.e., $f = \sum_k a_{ck} z^{k-1}$) or exponential function [i.e., $f = \sum_k a_{ck} \exp(b_{ck} z^{k-1})$] of a given degree. The results of the curve fitting process are the coefficients of the polynomial (or exponential) function, a_{ck}'s, and covariance matrix $COV(a_{ck}, a_{ck'})$, where $k = 1,2,\ldots,K$; the number of terms retained in the polynomial (or exponential) function. The elements of the covariance matrix are derived from the variances (uncertainties), σ_{ci}^2's.

2. Perform line-integration of the fitting curve between the breeding zone boundaries, Z1 and Z2. The integration yields the value C and its variance σ_C^2. The variance in the integrated value C is derived using the covariance matrix $COV(a_{ck}, a_{ck'})$.

3. Likewise, using the experimental data set, $\{z_i, e_i, \sigma_{ei}^2\}$, perform the above curve fitting procedures and line-integration to obtain the fitting coefficients a_{ek}'s, the covariance matrix $COV(a_{ek}, a_{ek'})$, the integrated value E, and its variance σ_E^2's.

4. The prediction uncertainty in the integrated TPR is quantified in terms of X_l where $X_l = (\chi - 1) \times 100$ and $\chi = C/E$. The relative variance in χ, σ_{lr}^2, is the algebraic sum of σ_{Cr}^2 and σ_{Er}^2; the relative variance in the integrated values C and E, respectively.

Because of the heterogeneities introduced in the WCC experiment, the breeding zone has three distinct subzones (a subzone behind each coolant channel). The relationship between the $(C/E)_j$ value of the integrated TPR and the associated variance in each subzone j and the overall calculated-to-experimental (C/E) value of the integrated TPR and its variance in the entire breeding zone is derived as follows:

If the breeding zone is divided into several subzones, j, where $j = 1,2,\ldots,J$, the C/E values for the integrated TPR in the entire breeding zone is given by

$$\left(\frac{C}{E}\right) = \frac{\sum_{j=1}^{J} C_j}{\sum_{j=1}^{J} E_j} = \frac{\sum_{j=1}^{J} \left(\frac{C_j}{E_j}\right) E_j}{\sum_{j=1}^{J} E_j} = \sum_{j=1}^{J} \left(\frac{C_j}{E_j}\right) \omega_{Ej} \ , \tag{6}$$

where

$$\omega_{Ej} = \frac{E_j}{\sum_{j=1}^{J} E_j} \tag{7}$$

and is defined as the fractional contribution of zone j to the total line-integrated TPR obtained from the experimental data set. Denoting,

$$\sigma_C^2 \equiv \text{variance in } C = \sum_{j=1}^{J} C_j$$

and

$$\sigma_E^2 \equiv \text{variance in } E = \sum_{j=1}^{J} E_j \ , \tag{8}$$

we have

$$\sigma_C^2 = \sum_{j=1}^{J} \sigma_{Cj}^2 \quad \text{and} \quad \sigma_E^2 = \sum_{j=1}^{J} \sigma_{Ej}^2 \ , \tag{9}$$

where the variances σ_{Cj}^2's (and σ_{Ej}^2's) are assumed uncorrelated among subzones. The relative variance in C/E of the total integrated TPR is then given by

$$\sigma_{Ir}^2 = \sigma_{Cr}^2 + \sigma_{Er}^2 = \frac{\sum_{j=1}^{J} \sigma_{Cj}^2}{C^2} + \frac{\sum_{j=1}^{J} \sigma_{Ej}^2}{E^2}$$

$$= \frac{\sum_{j=1}^{J} \frac{\sigma_{Cj}^2}{C_j^2} \cdot C_j^2}{C^2} + \frac{\sum_{j=1}^{J} \frac{\sigma_{Ej}^2}{E_j^2} \cdot E_j^2}{E^2}$$

$$= \sum_{j=1}^{J} \sigma_{Cjr}^2 \cdot \omega_{Cj}^2 + \sum_{j=1}^{J} \sigma_{Ejr}^2 \cdot \omega_{Ej}^2 \ , \tag{10}$$

where

$\sigma_{Cr}^2 \equiv$ relative variance of C

$\sigma_{Er}^2 \equiv$ relative variance of E

$\sigma_{Cjr}^2 \equiv$ relative variance of C_j

$\sigma_{Ejr}^2 \equiv$ relative variance of E_j

$\omega_{Cj} \equiv$ fractional contribution of zone j to the line-integrated TPR obtained from the calculation data set.

But, the relative variance in (C_j/E_j), σ_{jr}^2 is given by

$$\sigma_{jr}^2 = \sigma_{Cjr}^2 + \sigma_{Ejr}^2 \ . \tag{11}$$

Thus, Eq. (10) becomes

$$\sigma_{Ir}^2 = \sum_{j=1}^{J} (\sigma_{jr}^2 - \sigma_{Ejr}^2) \cdot \omega_{Cj}^2 + \sum_{j=1}^{J} \sigma_{Ejr}^2 \omega_{Ej}^2$$

$$= \sum_{j=1}^{J} \sigma_{jr}^2 \cdot \omega_{Cj}^2 + \sum_{j=1}^{J} \sigma_{Ejr}^2 (\omega_{Ej}^2 - \omega_{Cj}^2) \ . \tag{12}$$

However, we have

$$\omega_{Cj}^2 \approx \omega_{Ej}^2 \ . \tag{13}$$

Therefore, the relative variance in the C/E value of the overall integrated TPR, σ_{Ir}^2, could be expressed in terms of the relative variance in the C/E value of subzonal integrated TPR, σ_{jr}^2, as follows:

$$\sigma_{Ir}^2 \approx \sum_{j=1}^{J} \sigma_{jr}^2 \cdot \omega_{Ej}^2 \ . \tag{14}$$

In the BEO experiment, zonal TPR were measured inside several subzones that are relatively small ($\Delta z = \sim 5$ cm). In this special case, the measured (and the corresponding calculated) local TPR, e_j, (and c_j) are derived as constant values over a given subzone j. The C/E value of the line integrated TPR in the total system, given by Eq. (6), is now expressed as

$$\frac{C}{E} = \frac{\sum_j c_j \Delta z_j}{\sum_j e_j \Delta z_j} \ , \tag{15}$$

where Δz_j is the subzone width in z direction. The relative variance of C/E, σ_{Ir}^2, given by Eq. (10), can be obtained using the following expressions:

$$\sigma_{Cjr}^2 = (c_j \sigma_{cjr} \Delta z_j)^2 / C^2 \ , \quad \sigma_{Ejr}^2 = (e_j \sigma_{ejr} \Delta z_j)^2 / E^2 \ , \tag{16}$$

$$\omega_{Cj}^2 = (c_j \Delta z_j)^2 / C^2 \ , \qquad \omega_{Ej}^2 = (e_j \Delta z_j)^2 / E^2 \ , \tag{17}$$

where the local values c_j and e_j are used whose relative standard deviations are σ_{cjr} and σ_{ejr}, respectively. In addition, in the case where the calculated local TPR from natural lithium, c_{nj}, is derived from local TPR from Li-6 and Li-7, c_{6j} and c_{7j}, respectively (e_{nj}, e_{6j}, and e_{7j} for the experimental data), the following applied:

$$c_{nj} = a_6 c_{6j} + a_7 c_{7j} \ , \qquad e_{nj} = a_6 e_{6j} + a_7 c_{7j} \tag{18}$$

$$\sigma_{c_{nj}}^2 = a_6^2 \sigma_{c_{6j}}^2 + a_7^2 \sigma_{c_{7j}}^2 \ , \quad \sigma_{e_{nj}}^2 = a_6^2 \sigma_{e_{6j}}^2 + a_7^2 \sigma_{e_{7j}}^2 \ , \tag{19}$$

where a_6 and a_7 are the enrichment of Li-6 (0.0742) and Li-7 (0.9258) in natural lithium, and $\sigma_{c_{6j}}^2$ and $\sigma_{c_{7j}}^2$ are the variance in the local values c_{6j} and c_{7j}. Likewise, the variance in the local values e_{6j}, and e_{7j} are $\sigma_{e_{6j}}^2$ and $\sigma_{e_{7j}}^2$. The relative variance, σ_{njr}^2, of the calculated-to-experimental value, c_{nj}/e_{nj}, is then given by

$$\sigma_{njr}^2 = \sigma_{c_{njr}}^2 + \sigma_{e_{njr}}^2 \ , \tag{20}$$

where the relative variances, $\sigma_{c_{njr}}^2$ and $\sigma_{e_{njr}}^2$, are given by

$$\sigma_{c_{njr}}^2 = \sigma_{c_{nj}}^2 / c_{nj}^2 \ , \quad \sigma_{e_{njr}}^2 = \sigma_{e_{nj}}^2 / e_{nj}^2 \ . \tag{21}$$

The prediction uncertainty in the integrated TPR from natural lithium {expressed in terms of the quantity $\{[(C_n/E_n) - 1] \times 100\}$ can also be estimated in the same manner from the prediction uncertainties in the integrated T_6 and T_7 measured by Li-glass and NE213 detectors, respectively. The governing expressions in this case are similar to those given by Eqs. (18) through (21), i.e.,

$$C_n = a_6 C_6 + a_7 C_7 \ , \qquad E_n = a_6 E_6 + a_7 E_7 \tag{22}$$

$$\sigma_{C_n}^2 = a_6^2 \sigma_{C_6}^2 + a_7^2 \sigma_{C_7}^2 \ , \quad \sigma_{E_n}^2 = a_6^2 \sigma_{E_6}^2 + a_7^2 \sigma_{E_7}^2 \tag{23}$$

$$\sigma_{nr}^2 = \sigma_{C_{nr}}^2 + \sigma_{E_{nr}}^2 \tag{24}$$

$$\sigma_{C_{nr}}^2 = \sigma_{C_n}^2 / C_n^2 \ , \qquad \sigma_{E_{nr}}^2 = \sigma_{E_n}^2 / E_n^2 \ , \tag{25}$$

where the integrated quantities, C_6, C_7, E_6, and E_7 are used instead.

V. ANALYTICAL RESULTS AND COMPARISON WITH EXPERIMENTAL VALUES

V.A. WCC Experiment

The neutron spectrum inside and around the coolant channels has an appreciable low-energy neutron component due to neutron moderation by the coolant (containing hydrogen). Consequently, reactions that have a large absorption cross-section at low-energy neutrons are noticeably large around these heterogeneities. Figure 3 (based on DOT 5.1 calculations) shows the T_6 and T_7 profiles along the central axis where spikes are apparent in the case of T_6 around these channels. The T_6 profile is very steep at the boundaries of Li_2O/WCC with local increase by a factor of 4 to 6. The axial profile of the $^{197}Au(n,\gamma)$ reaction is very similar in shape to the T_6 profile. Since T_7 is only sensitive to the high-energy component of the neutron spectrum, the sudden change in local values does not exist in the T_7 profiles. This is also true for reactions that have high threshold energies.

V.A.1. Prediction Uncertainty of TPR from Li-6 and Nonthreshold Reactions

Figures 4 and 5 show the $(c/e)_i$ of the local values for the $^{197}Au(n,\gamma)$ and $^{6}Li(n,\alpha)t$ reactions where noticeable changes in the values occur near coolant channels (at depth of ~10 and 30 cm) and at the Li_2O/Li_2CO_3 boundaries. Systematic differences appear between the Monte Carlo and Sn calculations and the statistical errors in the former are large and overlapping. The values shown in Fig. 5 are based on T_6 measurements performed by the Li-glass detectors (numerical values of the prediction uncertainty of T_6 are given in Table II). With the Li-foil detectors, less discrepancy between calculations and measurements were observed for T_6. The $(c/e)_i$ values in this case are, on the average, lower than those obtained with the Li-glass detectors by ~5 to 10% (closer c/e values to unity). This can be seen from Fig. 6 where the calculations are those obtained by DOT 5.1/MATXS6D. Except for the second data point located just behind the coolant channel of the first wall, the $(c/e)_i$ values are 0.95 to 1.1 in the

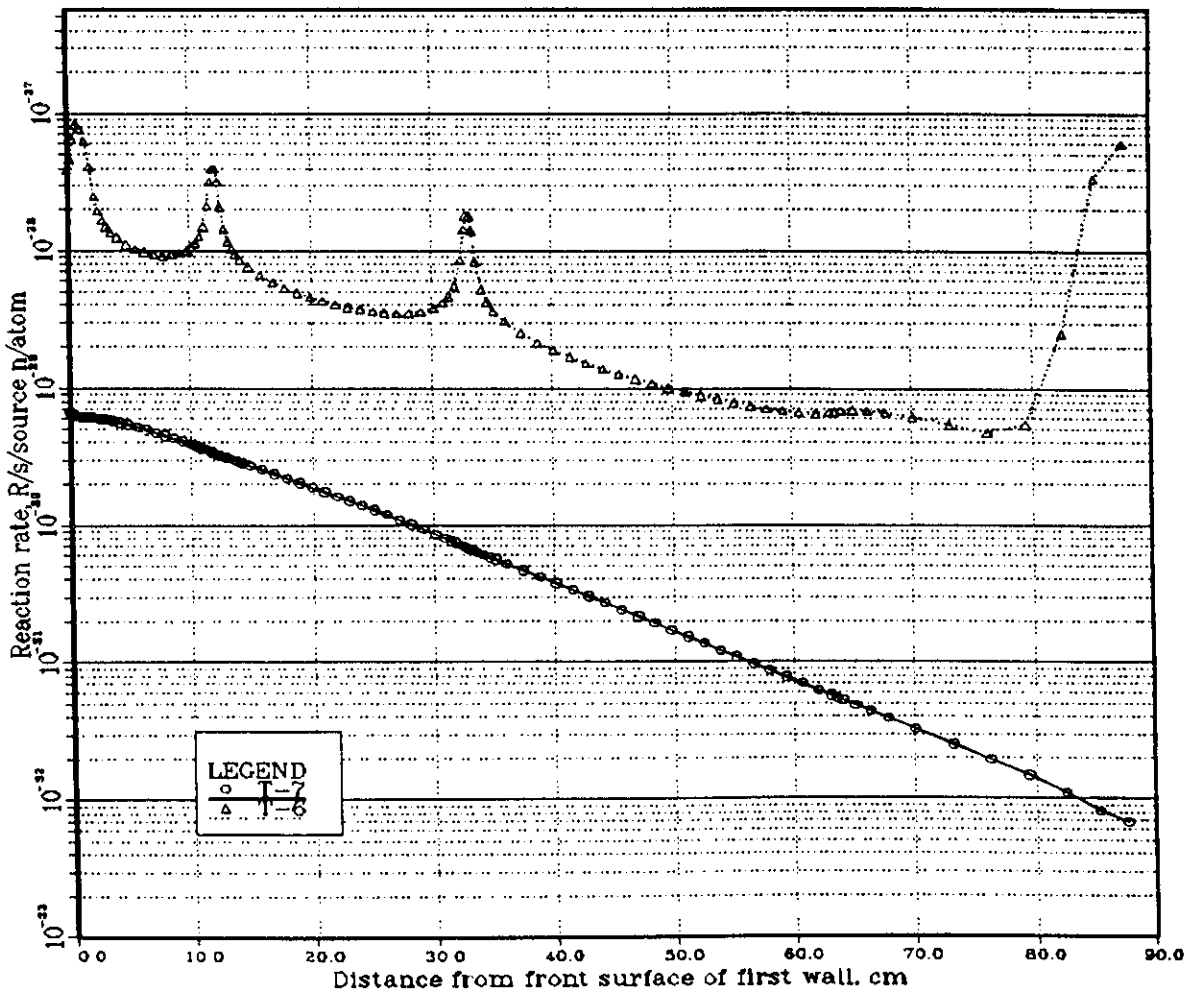

Fig. 3. The T_6 and T_7 production rates along the central axis (WCC experiment).

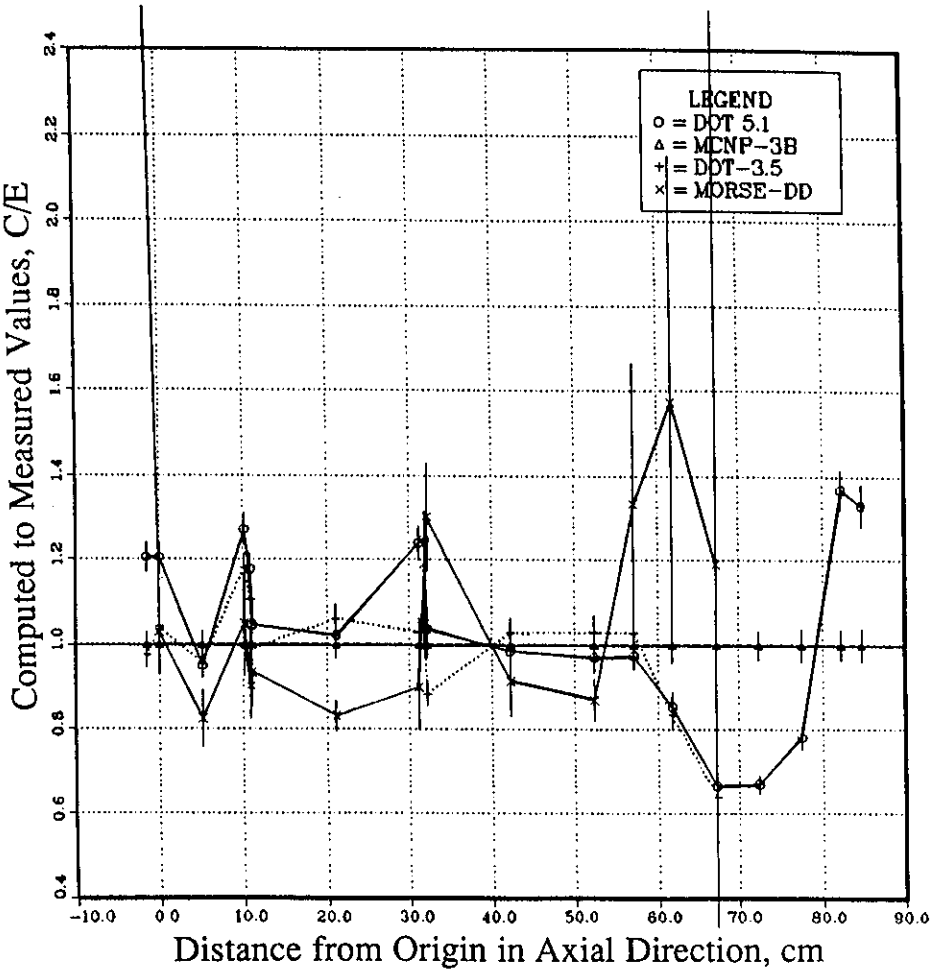

Fig. 4. The $(c/e)_i$ values of the Au-197(n,γ)Au-198 reaction rate along the off-central axis (WCC experiment).

bulk of the Li_2O zone (the first data point is at the front of the first wall).

To assess the prediction uncertainty in line-integrated TPR, we first consider the measurements taken by the Li-glass detectors whose number is thirteen as shown in Table II. Two measurements, seven measurements, and four measurements were taken in the first, second and third breeding zones that follow each coolant channel. These three zones were divided into five subzones whose boundaries and other line-integration details are shown in Table III. The line integration was not extended beyond the integration boundaries shown in Table III since the fitted curves could have profiles that are not realistic due to the absence of measured data beyond these boundaries. The choice of a polynomial or exponential fitting depends on the steepness of the TPR profile in a given subzone. Some data at locations lying in other subzones were used when the fitting curve was derived in a particular subzone. However, integrating the obtained curve was only performed between the integration boundaries.

Figure 7 shows the fitting curves for the experimental and calculated data sets obtained from the discrete ordinates codes (similar curves were obtained from the Monte Carlo codes, not shown). The calculational and experimental errors are shown at each data point. Tables IV and V give the prediction uncertainty (defined in terms of $[\{(Cj/Ej) - 1\} \times 100]$ and the relative standard deviation in the Cj/Ej value of the integrated T_6, σ_{jr}, in each subzone, j, and in the total breeding zone. Also given are the parameters ω_{Cj}, ω_{Ej}, $(Cj/Ej)\omega_{Ej}$, and $\sigma_{jr}^2\omega_{Ej}^2$ along with the corresponding parameters for the total system as defined by Eqs. (6) through (14). From these Tables one can notice the following:

1. The fractional contributions to the total integrated TPR from each subzone, ω_{Cj}'s and ω_{Ej}'s, are very similar regardless of the calculational methods used which justifies the assumption given by Eq. (13). The difference, however, is in the absolute value of the integrated TPR in each subzone and in the total system. In DOT calculations, the integrated TPR, C, in the

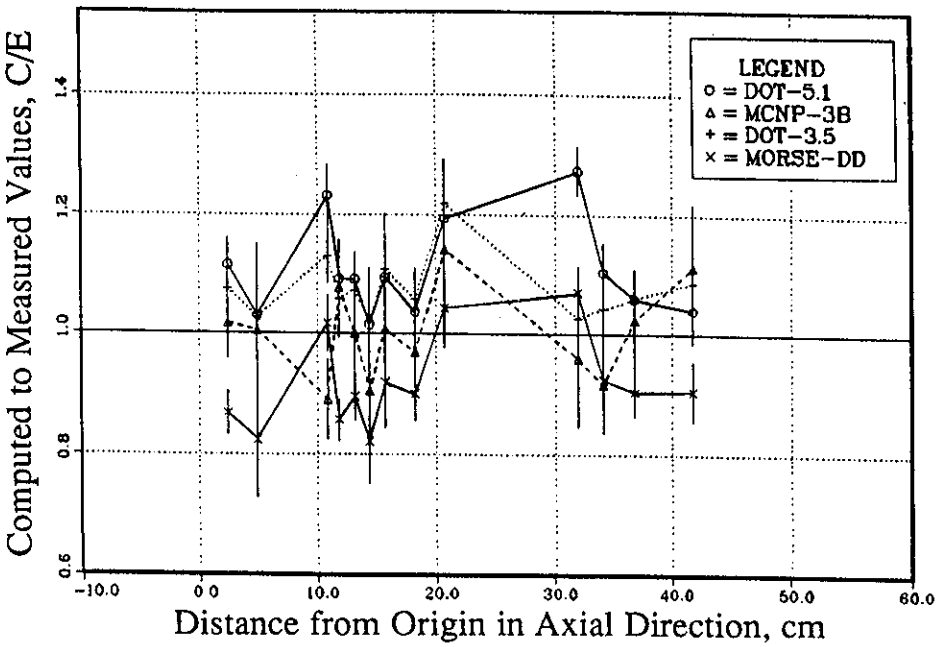

Fig. 5. The $(c/e)_i$ values of TPR from Li-6 (T_6) measured by Li-glass detectors along the central axis (WCC experiment).

U.S. calculations is larger than that obtained by JAERI, leading to prediction uncertainties of *10.5 and 7.2%*, respectively. The relative standard deviation, σ_{Ir}, given by Eq. (14), is *2.2%* in both cases. This is because no account was made to uncertainties due to data/method approximations in DOT calculations and the relative standard deviation, σ_r, accounts only for the experimental errors.[a] This is not the case in the Monte Carlo calculations where the calculational statistical errors in local TPR were considered. The larger c_i values in the U.S. calculations performed by MCNP shown in Fig. 5 are also reflected in Table V where the prediction uncertainty in the total integrated TPR is ~0.4% (U.S.) and −10.5% (JAERI). The corresponding relative standard deviations are *2.8 and 2.3%*, respectively.

2. The relative standard deviation, σ_{Ir}, seems to be always smaller than the relative standard deviation in each subzone, σ_{jr}. The zone with the largest $\sigma_{jr}^2\omega_{Ej}^2$ value (subzone a in our case) will have the largest contribution to σ_{Ir} [see Eq. (14)].

3. The largest contribution to the total integrated value, C (and integrated value E), comes from the first subzone a, which is the closest subzone to the incident neutron source, and this contribution is ~42% over a depth of only 7 cm. The second largest contribution is from subzone c (25%), which has a width of ~8.9 cm. Note that the contribution from subzone b (T_6 profile is steep) is ~16% over a depth of only 2.3 cm. Since the C/E of the total integrated TPR is expressed by Eq. (6), the subzone with the largest $(Cj/Ej)\omega_{Ej}$ value will have the largest contribution to C/E (subzone a in our case).

Figure 8 shows in graphical forms the integrated TPR in each subzone and in the system. Also shown is the integrated TPR, C(j), as obtained directly from the T_6 profile calculated by the DOT5.1 code and shown in Fig. 3. Since the first spike behind the first

[a]Previous work has indicated that the uncertainty in local T_6 and T_7 due to uncertainties in nuclear data is 2 to 4% and 4 to 6%, respectively.[33] These uncertainties could be larger (by 9%) when the uncertainties in the secondary energy distribution (SED) are accounted for.[34] To be noted is that the uncertainties in the integrated TBR in several candidate blanket concepts due to data uncertainties were found to be 2 to 5% (Ref. 35). In addition, and with regard to the discrete ordinates (DO) method, other sources of uncertainties could contribute to the overall uncertainties in the calculated TPR such as the number of energy group considered, the size of the spatial mesh, the quadrature set and the order of the Legendre polynomials used to describe the cross-section data. Recent analysis has indicated[36,37] that the discrepancies between results based on coarse group versus fine group could be as large as ~20%. Likewise coarse spatial mesh influences low-energy neutron flux by ~20% at maximum. Other discretization parameters have small influence by 1 to 2%. On the other hand, results from low number of history (~10^4) in the Monte Carlo (MC) calculations can deviate from results based on large number of history (~10^8) by as large as 80% (Ref. 36). The results reported here, however are based on fine group/mesh/quadrature sets in the DO method and for large number of histories in the MC calculations.

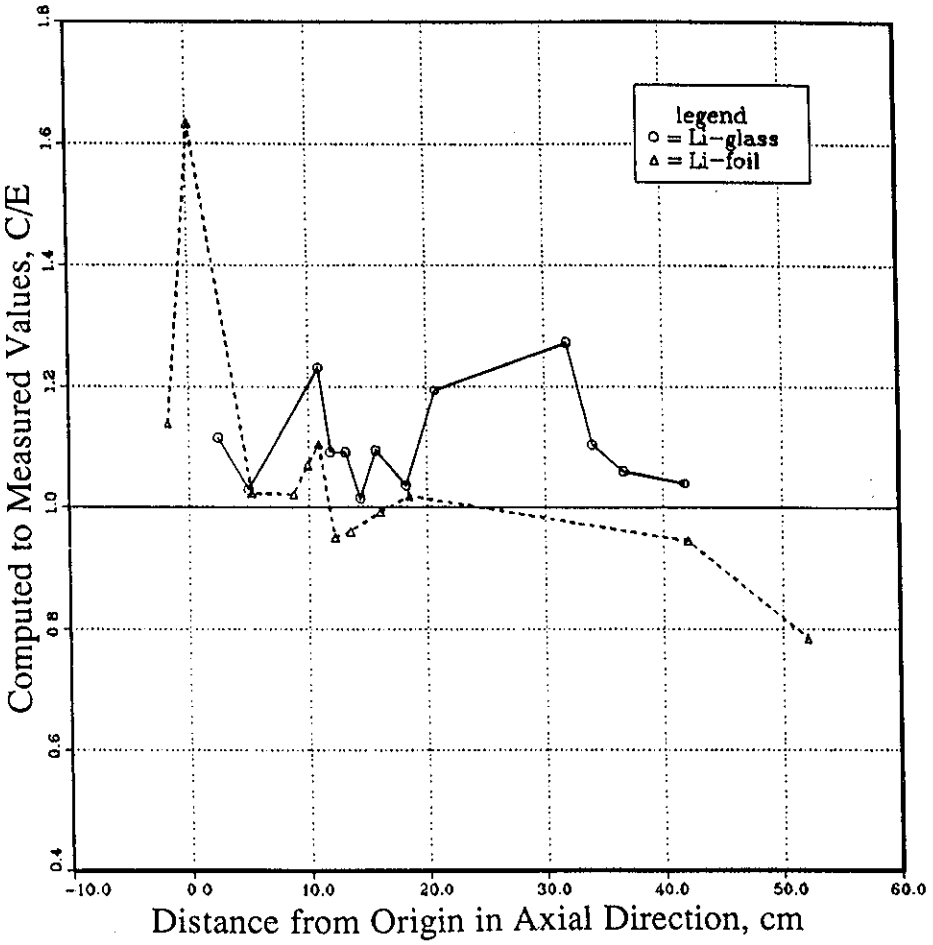

Fig. 6. The $(c/e)_i$ values of TPR from Li-6 (T_6) measured by two detectors along the central axis (WCC experiment).

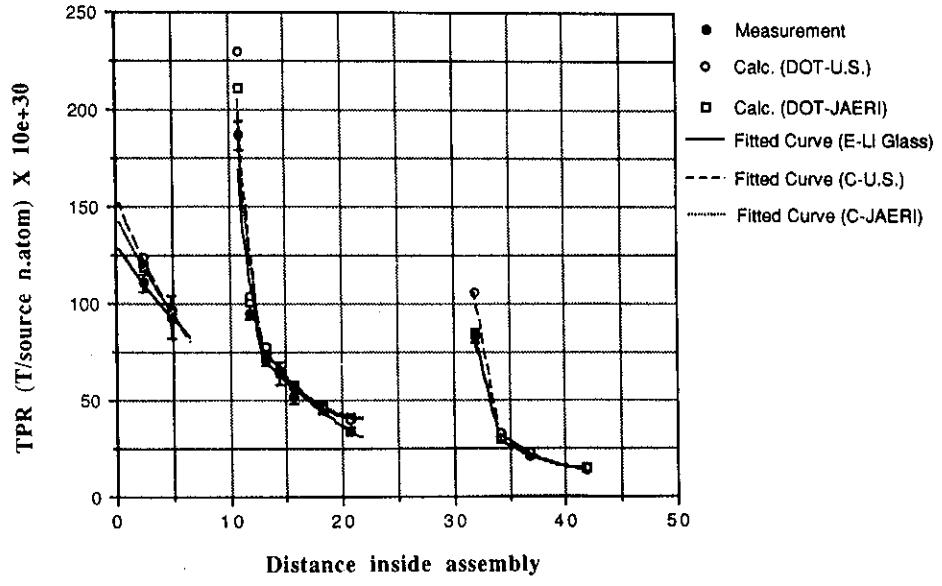

Fig. 7. Calculational and experimental data sets and the fitting curves for T_6 measured by Li-glass detectors in the WCC experiment (DOT calculations).

TABLE II

Calculated-to-Experimental Values for T_6 Along the Central Axis in the WCC Experiment

(Measurements by Li-glass detectors)

Position	Z (cm)[a]	Measured Value	Experimental Error (%)	C/E Values					
				U.S.			JAERI		
				DOT 5.1	MCNP	S.E. (%)[c]	DOT 3.5	MORSE-DD	S.E. (%)[c]
1	2.40	1.107−28[b]	4.09	1.116	1.018	5.86	1.075	0.868	4.36
2	4.93	9.288−29	11.82	1.031	1.006	12.57	1.028	0.824	11.89
3	10.87	1.867−28	4.14	1.232	0.891	7.53	1.131	1.018	4.68
4	11.88	9.529−29	3.78	1.092	1.077	7.69	1.059	0.857	4.03
5	13.15	7.136−29	4.32	1.091	1.001	6.31	1.074	0.896	4.50
6	14.41	6.399−29	8.69	1.016	0.906	9.56	1.022	0.822	8.74
7	15.68	5.180−29	8.26	1.095	1.009	9.31	1.110	0.919	8.30
8	18.21	4.480−29	5.04	1.038	0.969	6.82	1.058	0.900	5.10
9	20.75	3.371−29	6.27	1.194	1.142	7.72	1.218	1.044	6.34
10	31.95	8.294−29	3.11	1.274	0.960	12.00	1.028	1.070	4.20
11	34.13	2.976−29	4.44	1.105	0.916	8.80	1.043	0.924	4.72
12	36.176	2.132−29	4.37	1.060	1.024	8.42	1.060	0.904	4.50
13	41.82	1.412−29	5.40	1.040	1.113	9.6	1.088	0.905	5.55

[a]Measured from the front edge of the Li_2O located behind the FW/PE layer. This edge is at a distance of 76.87 cm from D-T point source.

[b]Read as 1.107×10^{-28}.

[c]$\sqrt{(\text{experimental error})^2 + (\text{Monte Carlo statistical error})^2}$.

wall is not shown in the curve-fitting results of the DOT5.1 calculation due to the absence of measuring points just behind the first wall (see Fig. 7), the integrated TPR in subzone a, C(j), is underestimated by as much as ~17% relative to C(j), but the overall TPR is underestimated by ~4.4% in the total system.

These procedures were also applied to the calculation and experimental values of local TPR obtained by the Li-foil detectors. Five subzones were considered, namely subzones a, f, b, c, d'. The line integration boundaries, locations of spatial points considered in the integration, and other details of the curve fitting procedures are described in Table III. Note that boundaries of subzones a, b, and c are the same as those considered in the case of the Li-glass measurements and that subzone d' has the same boundaries as zone d and e combined.

Figure 9 and Table VI show the fitting curves and the pertaining parameters of the experimental and calculated data as obtained by JAERI and the U.S. using the discrete ordinates codes. Again, one can notice that the weighting coefficients ϖ_{Cj} and ϖ_{Ej} are similar although the similarity is not quite the same as that in the case of the Li-glass measurements. The integrated quantities C and E in the total system are much larger than those given in Table IV due to (a) the inclusion of subzone f, and (b) the steepness of the fitting curve in zone a behind the first coolant channel as shown in Fig. 9. The observations (1) to (3) cited earlier still hold in this case. The prediction uncertainties in T_6 are *14.2% (U.S.) and 7.5% (JAERI)* with relative standard

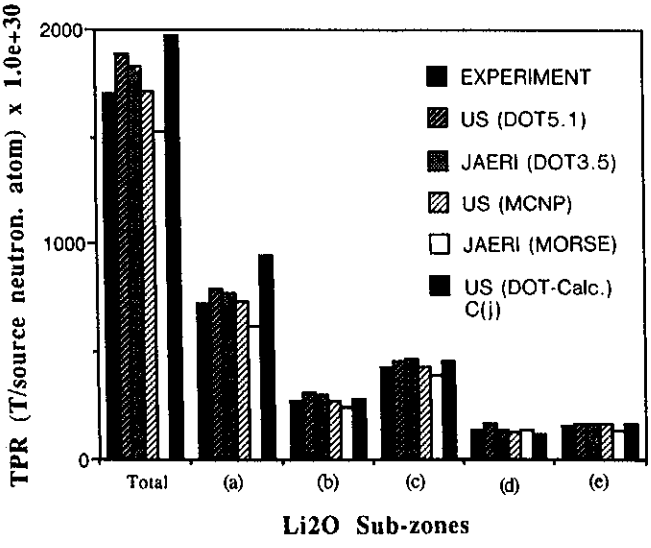

Fig. 8. Line integrated TPR from Li-6 in each subzone and in the system of the water coolant channel experiment.

TABLE III

Description of Parameters Used in the Line Integration Analysis of TPR in the WCC Experiment

	Li-Glass Measurement				
	Subzones				
	a	b	c	d	e
Number of locations of measurements within subzone	2	3	4	2	2
Number of locations considered in curve fitting	2	3	5	2	3
Depth (z) of locations considered in curve fitting (cm)	2.4, 4.93	10.87, 11.88, 13.15	13.15, 14.14, 15.68, 18.21, 20.74	31.95, 34.13	34.13, 36.76, 41.82
Boundaries of subzone integration (z1,z2) (cm)	0 to 7.0	10.75 to 13.15	13.15 to 22.0	31.83 to 34.13	34.13 to 42.0
Type of fitting	E[a]	E	P[b]	P	P
Number of terms retained in curve fitting	2	2	3	2	3
	Li-Foil Measurement				
	Subzones				
	a	f	b	c	d′
Number of locations of measurements within subzone	2	2	3	3	2
Number of locations considered in curve fitting	2	2	3	3	2
Depth (z) of locations considered in curve fitting (cm)	0.15, 5.15	8.75, 9.9	10.9, 12.2, 13.5	13.5, 16.0, 18.5	42.0, 52.0
Boundaries of subzone integration (z1,z2) (cm)	0.0 to 7.0	8.75 to 9.9	10.75 to 13.15	13.15 to 22	31.83 to 42.0
Type of fitting	E	E	E	P	P
Number of terms retained in curve fitting	2	2	2	3	2

[a]Exponential fitting.
[b]Polynomial fitting.

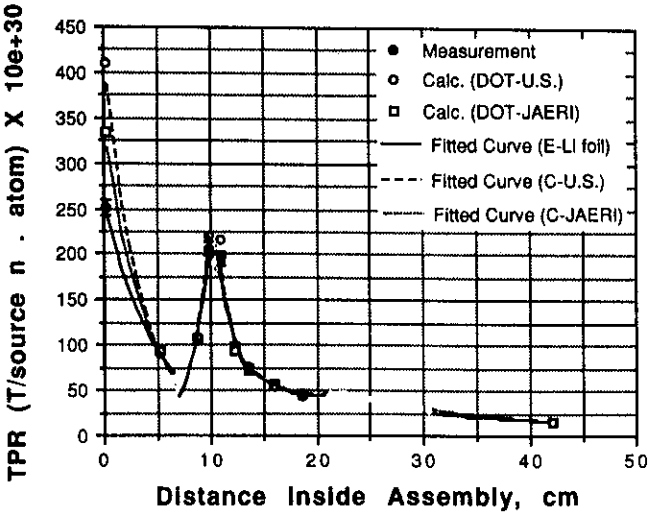

Fig. 9. Calculational and experimental data sets and the fitting curves for T_6 measured by Li-foil detectors in the WCC experiment (DOT calculations).

deviations of *1.5%* in both cases. The steepness in the T_6's fitting curve just behind the first coolant channel is due to the fact that a measuring location at z = 0.15 cm was considered in the analysis. This is not the case with the Li-glass measurements where the first measuring location is at a depth of z = 2.4 cm. Likewise, no steepness was observed in the fitting curve behind the third coolant channel in the Li-foil case due to the same reason. To have a fair comparison between the results of the Li-glass and Li-foil measurements, the analysis was carried out without considering subzone f in the Li-foil case and augmenting subzones d and e in the case of the Li-glass measurements. Table VII shows this comparison. The coefficients ϖ_{Ej}'s are similar for subzones b and c but are different for subzones a and d′. While subzone a contributes ~42% to the total integrated TPR in the Li-glass case, this contribution is ~50% in the Li-foil case. This is due to the lack of a measuring location just behind the first coolant channel in the Li-glass case, which would have reflected a

TABLE IV

Comparison Between the Prediction Uncertainty of TPR from Li-6 (T_6) in Each Subzone and in the Total System of the WCC Experiment

(Discrete ordinates calculation – Li-glass measurements)

Zone Thickness (cm)		C_j	$\bar{\omega}_{Cj}$	E_j	$\bar{\omega}_{Ej}$	$C_j/E_j - 1 \times 100$	σ_{jr} (%)	$(C_j/E_j)\bar{\omega}_{Ej}$	$\sigma_{jr}^2\bar{\omega}_{Ej}^2$
JAERI									
a	7	769[a]	0.42	725	0.42	6.1	4.7	0.446	3.897
b	2.4	298	0.16	270	0.16	10.4	2.4	0.177	0.147
c	8.85	461	0.25	424	0.25	8.7	2.8	0.272	0.490
d	2.3	137	0.08	133	0.08	3.0	2.6	0.082	0.043
e	7.87	164	0.09	154	0.09	6.5	3.6	0.096	0.105
Total system		1829	1.00	1705	1.00	7.2	2.2		
U.S.									
a	7	790	0.42	725	0.42	8.9	4.7	0.457	3.897
b	2.4	313	0.17	270	0.16	16.1	2.4	0.186	0.147
c	8.85	455	0.24	424	0.25	7.4	2.8	0.269	0.490
d	2.3	164	0.09	133	0.08	23.3	2.6	0.099	0.043
e	7.87	162	0.08	154	0.09	5.7	3.6	0.095	0.105
Total system		1884	1.00	1705	1.00	10.5	2.2	0.194	

[a]Units: [T atom·cm/Li atom/source neutron] $\times 10^{30}$.

TABLE V

Comparison Between the Prediction Uncertainty of TPR from Li-6 (T_6) in Each Subzone and in the Total System of the WCC Experiment

(Monte Carlo calculation – Li-glass measurements)

Zone Thickness (cm)		C_j	$\bar{\omega}_{Cj}$	E_j	$\bar{\omega}_{Ej}$	$C_j/E_j - 1 \times 100$	σ_{jr} (%)	$(C_j/E_j)\bar{\omega}_{Ej}$	$\sigma_{jr}^2\bar{\omega}_{Ej}^2$
JAERI									
a	7	619[a]	0.41	725	0.42	−14.5	4.9	0.359	4.235
b	2.4	242	0.16	270	0.16	−10.2	2.7	0.144	0.187
c	8.85	387	0.25	424	0.25	−8.7	2.8	0.228	0.490
d	2.3	138	0.09	133	0.08	3.5	3.6	0.083	0.083
e	7.87	139	0.09	154	0.09	−9.5	3.8	0.072	0.092
Total system		1525	1.00	1705	1.00	−10.5	2.3		
U.S.									
a	7	736	0.43	725	0.42	1.5	5.7	0.426	5.731
b	2.4	268	0.16	270	0.16	−0.48	4.3	0.159	0.473
c	8.85	421	0.25	424	0.25	−0.57	3.5	0.249	0.766
d	2.3	126	0.07	133	0.08	−5.0	9.4	0.076	0.566
e	7.87	160	0.09	154	0.09	3.9	6.9	0.094	0.386
Total system		1711	1.00	1705	1.00	0.4	2.8		

[a]Units: [T atom·cm/Li atom/source neutron] $\times 10^{30}$.

TABLE VI

Comparison Between the Prediction Uncertainty of TPR from Li-6 (T_6) in Each Subzone and in the Total System of the WCC Experiment

(Discrete ordinates calculation – Li-foil measurements)

Zone	Thickness (cm)	C_j	$\bar{\omega}_{Cj}$	E_j	$\bar{\omega}_{Ej}$	$C_j/E_j - 1 \times 100$	σ_{jr} (%)	$(C_j/E_j)\bar{\omega}_{Ej}$	$\sigma_{jr}^2\bar{\omega}_{Ej}^2$
JAERI									
a	7	1136[a]	0.47	975	0.43	16.5	2.5	0.501	1.156
f	3.05	325	0.13	326	0.14	−0.26	3.0	0.140	0.176
b	8.85	302	0.12	309	0.14	−2.4	2.2	0.137	0.095
c	2.3	469	0.20	469	0.21	0.1	4.0	0.210	0.706
d′	7.87	206	0.08	190	0.08	8.9	5.7	0.087	0.208
Total system		2438	1.00	2269	1.00	7.5	1.5		
U.S.									
a	7	1270	0.49	975	0.43	30.3	2.5	0.560	1.156
f	3.05	336	0.13	326	0.14	3.0	3.0	0.144	0.176
b	8.85	317	0.12	309	0.14	2.7	2.2	0.144	0.095
c	2.3	468	0.19	469	0.21	−0.25	4.0	0.209	0.706
d′	7.87	198	0.07	190	0.08	4.7	5.7	0.084	0.208
Total system		2589	1.00	2269	1.00	14.2	1.5		

[a]Units: [T atom·cm/Li atom/source neutron] × 10^{30}.

steepness in the fitting curve and hence larger values of integrated TPR at the first subzone a. The situation is reversed in subzone d′ where the contribution to the total integrated TPR is ~17% in the Li-glass case, whereas it is ~10% in the Li-foil case due to the lack of a measuring location just behind the third coolant channel in the Li-foil case. The integrated TPR in the total system is larger in the Li-foil case than in the Li-glass case

TABLE VII

Comparison Between the Prediction Uncertainty of TPR from Li-6 (T_6) in the WCC Experiment Using Two Different Measuring Techniques

(Discrete ordinates calculations – U.S.)

Zone	Thickness (cm)	Li-Foil						Li-Glass					
		C_j	$\bar{\omega}_{Cj}$	E_j	$\bar{\omega}_{Ej}$	$C_j/E_j - 1 \times 100$	σ_{jr} (%)	C_j	$\bar{\omega}_{Cj}$	E_j	$\bar{\omega}_{Ej}$	$C_j/E_j - 1 \times 100$	σ_{jr} (%)
a	7	1270[a]	0.56	975	0.50	30.3	2.5	790	0.42	725	0.42	8.9	4.7
b	2.4	317	0.14	309	0.16	2.7	2.2	313	0.17	270	0.16	16.1	2.41
c	8.85	468	0.21	469	0.24	−0.25	4.0	455	0.24	424	0.25	7.4	2.8
d′ (or) d + e	10.2	198	0.09	190	0.10	4.7	5.7	326	0.17	287	0.17	13.5[b]	2.3[c]
Total system		2253	1.00	1943	1.00	18.9	1.7[d]	1884	1.00	1705	1.00	10.5	2.2

[a]Units: [T atom·cm/Li atom/source neutron] × 10^{30}.
[b]Estimated from Eq. (6) where subzones d and e are considered.
[c]Estimated from Eq. (14) where subzones d and e are considered.
[d]Estimated from Eq. (14) where subzones a, b, c, d′ are considered.

TABLE VIII

Comparison Between the Prediction Uncertainty in Local and Integrated TPR from Li-6

(Based on discrete ordinates calculations)

	U.S.	JAERI
WCC Experiment		
Integrated TPR		
Li-glass	10.5[a] (2.2[b])	7.2 (2.2)
Li-foil (with zone f)	14.2 (1.5)	7.5 (1.5)
Li-foil (without zone f)	18.9 (1.7)	10.3 (1.7)
Local TPR		
Li-glass	12.5[c] (1.3[d])	~5.0 (1.3)
Li-foil	0.34 (1.4)	~0.2 (1.4)

[a]Prediction uncertainty, $X_I = [(C/E) - 1] \times 100$, obtained from Eq. (6).
[b]Relative standard deviation, σ_{Ir} (%), obtained from Eq. (14).
[c]Prediction uncertainty, $\bar{X}_I = [\bar{\chi}_I - 1] \times 100$, obtained from Eq. (5).
[d]Relative standard deviation, σ_{I_r} (%), obtained from Eq. (4).

since the contribution from subzone a is dominant. The integrated TPR is overpredicted by ~18.9% in the Li-foil case and by ~10.5% in the Li-glass case. The overprediction in the Li-foil case increased upon the exclusion of subzone f since this resulted in overemphasizing the contribution from subzone a in which the prediction uncertainty is ~30.3%. This large overestimation is due to the large $(c/e)_i$ value of local TPR just behind the first coolant channel [(c/e)i ~1.6] as seen in Fig. 6. The corresponding uncertainties in the total integrated TPR was also evaluated using JAERI's results. They are ~7.5% with σ_{Ir} = ~1.5% when subzone f is considered and ~10.3% with σ_{Ir} = ~1.7% when it is excluded. The same observations applied where the uncertainties increased as compared to the Li-glass case due to the reasons mentioned earlier. These results are summarized in Table VIII.

The prediction uncertainty in local and integrated TPR as obtained by both measuring techniques were compared. When Eqs. 1 to 5 are applied, it is estimated that the uncertainties in the local TPR from Li-6 based on DOT5.1 calculations are ~12.5 and 0.34% with the Li-glass and Li-foil measurements, respectively. The estimations in JAERI's calculations are ~5.0 and ~0.2%. The uncertainty in local and integrated TPR are comparable in the Li-glass case. This is not the case with the Li-foil measurements where the cancellation effect takes place between the local $(c/e)_i$ values that are larger than unity (at front locations) and those that are lower than unity at back locations (see Fig. 6). This demonstrates that uncertainties in the integrated TPR are driven by the uncertainties in local TPR at the front locations, which contribute most to the total integrated TPR.

Note from Table VIII that, on the average, the uncertainties in local and integrated TPR are larger by ~5 to 8% in the U.S. calculations as compared with the results obtained by JAERI. In Monte Carlo calculation, the JAERI's calculations are lower than that of the U.S. by ~8 to 10%, as shown in Table IX, for both the local and integrated TPR of the Li-glass measurements.

V.A.2. Prediction Uncertainty of TPR from Li-7

The $(c/e)_i$ values for local T_7 where measurements are performed by the NE213 indirect method are shown in Fig. 10. The value obtained by the U.S. (c/e ~1.1 to 1.25) are generally larger than those obtained by JAERI (c/e ~0.9 to 1.15). The overestimation (by ~10%) could be due to the $^7Li(n,n'\alpha)t$ cross section of JENDL3/PR2 (same as in JENDL3/PR1) used in folding the NE213 measured spectrum to estimate T_7. It was previously shown[3,6,8] from direct comparison between the JENDL3/PR1 (and /PR2) cross section for $^7Li(n,n'\alpha)t$ and Young's evaluation[38] used in the U.S. calculation that the former is lower than the latter by ~8 to 10% at 14 MeV. Thus, the experimental values obtained by the NE213 method could be lower than what they should be, which leads to the upward shift in the $(c/e)_i$ values. This is supported by the fact that the T_7 measurements by the Li-foil technique are lower than the NE213 measurements by ~10%. The prediction uncertainties in the local and integrated TPR from Li-6 and Li-7 are summarized in Table IX and depicted graphically in Figs. 11 and 12. The following can be observed:

For T_6 the following are observed:

1. The average local and integrated uncertainties are comparable (within a few percent) as long as the local $(c/e)_i$ values are comparable. Large deviation between them occurs (as is the case with the Li-foil measurements) when large local $(c/e)_i$ value(s) takes place at locations near the front surface of the breeding zone.

2. The uncertainties in both local and integrated TPR are larger in DOT calculations by ~10 to 15% than those obtained by the Monte Carlo method.

3. The uncertainties in T_6 estimated by the U.S. codes/data are larger than those estimated with JAERI's codes and data by ~10 to 15%.

4. The variances in the estimated uncertainties seem to be larger in the integrated TPR as compared to those associated with the average local TPR.

5. Considering the results of the U.S. and JAERI's calculations of the integrated TPR from Li-6 measured by Li-glass and Li-foil detectors, the extreme uncertainties (defined as the largest uncertainties possible, accounting for σ_{Ir}'s) are −13 to 21% (see Fig. 11). This leads to an uncertainty range of ~34%, about 10 to 15% of which is attributed to differences in codes/data

TABLE IX

The Prediction Uncertainties (%) in Local and Integrated TPR of the WCC Experiment

Items	U.S.		JAERI	
	DOT5.1	MCNP	DOT3.5	MORSE-DD
T_6				
Li-glass				
Local	12.5[a] (1.3)[b]	−0.5 (2.2)	−5.0 (1.3)	−8.6 (2.2)
Integrated	10.5 (2.2)	0.4 (2.8)	7.2 (2.2)	−10.5 (2.2)
Li-foil				
Local	0.34 (1.4)	---	−0.2 (1.4)	---
Integrated	18.9[c] (1.7)	---	10.3[c] (1.7)	---
T_7				
NE213				
Local	20.9 (2.5)	10.5 (2.9)	−9.2 (2.5)	−3.8 (2.9)
Integrated	20.7 (3.3)	9.3 (3.4)	4.2 (3.3)	4.9 (3.3)
Li-foil				
Local	7.7 (1.4)	---	−9.1 (1.4)	---
Integrated	7.8 (1.4)	---	−8.4 (1.4)	---

[a]Prediction uncertainty, $[(C/E) - 1] \times 100$.
[b]Relative standard deviation, σ_r (%).
[c]Excluding subzone f.

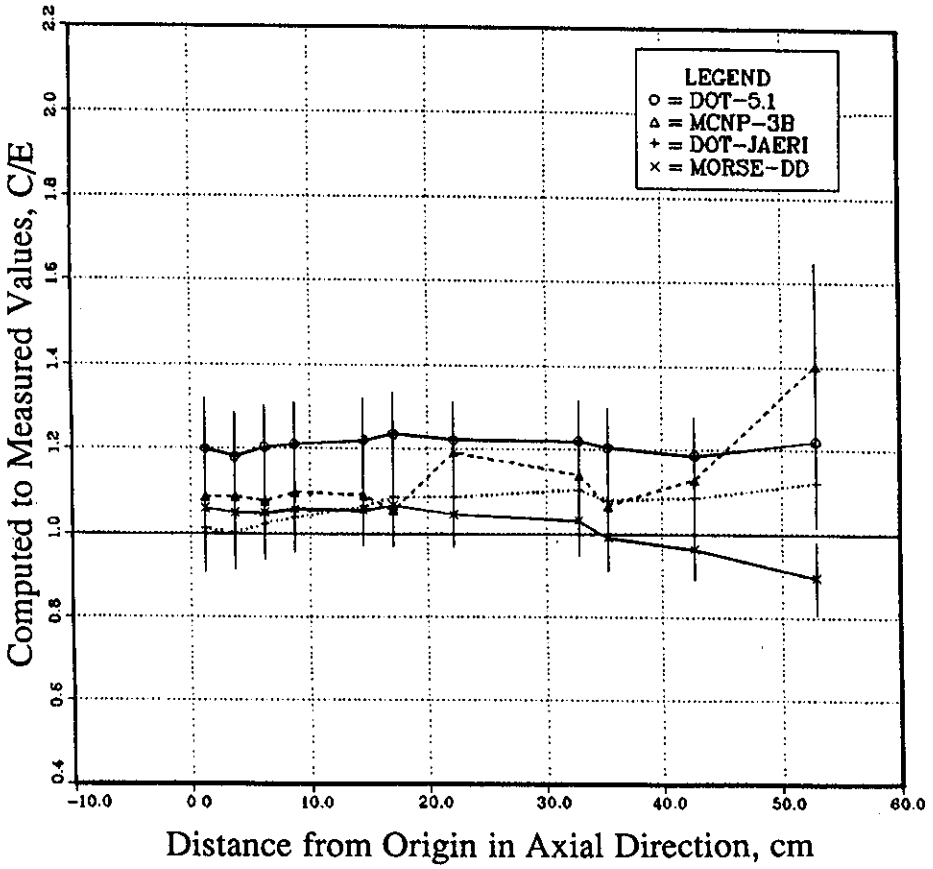

Fig. 10. The $(c/e)_i$ values of TPR from Li-7 (T_7) measured by NE213 detectors along the central axis (WCC experiment).

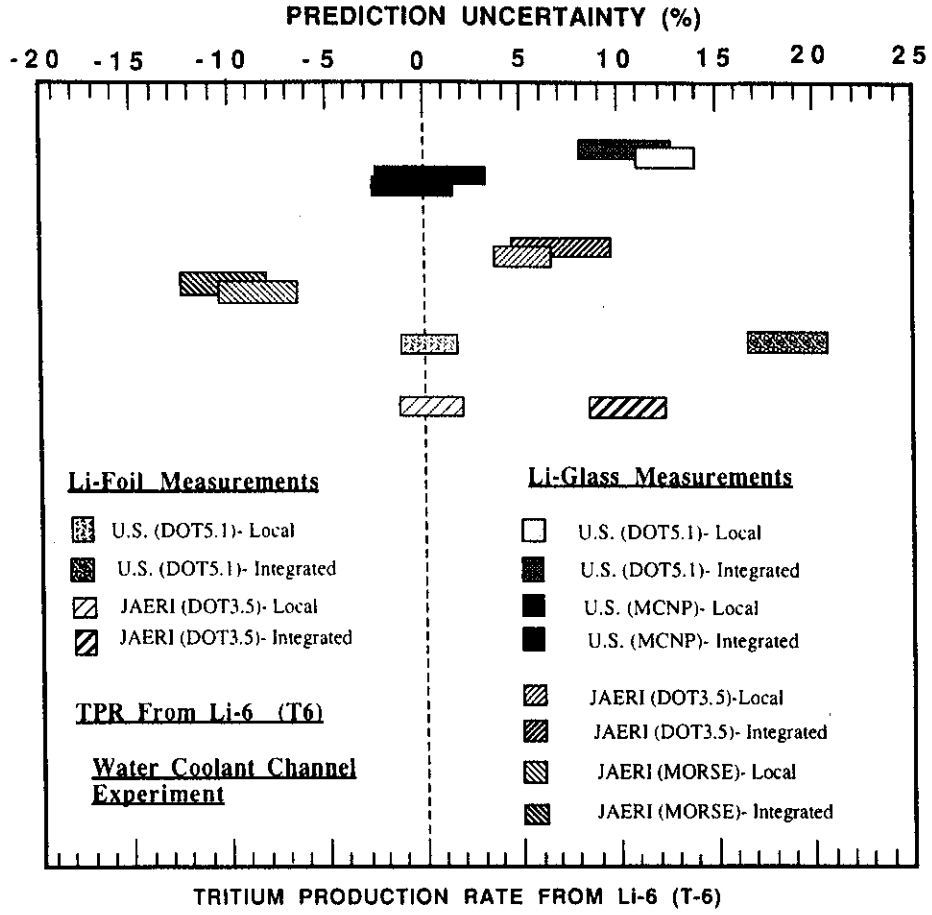

Fig. 11. The prediction uncertainties in local and integrated TPR from Li-6 in the WCC experiment.

and 10 to 18% is attributed to differences in measuring techniques. If only the U.S. data are considered, the extreme uncertainties vary from −2 to 21% (uncertainty range of ~23%), about 10% of which is attributed to differences in codes and ~13% is attributed to differences in measuring techniques.

For T_7 the following are observed:

1. The average local and integrated uncertainties are also comparable (within a few percent) as long as the local $(c/e)_i$ values are comparable. Also, the variances in local TPR are smaller than those associated with integrated TPR. The variances in both TPRs, however, are larger than those for T_6.

2. The uncertainties in T_7 estimated by the U.S. codes/data are larger than those estimated with JAERI's codes and data by ~15 to 18%.

3. The extremes in the uncertainties of the integrated TPR are −10 to 24% (see Fig. 12). This leads to an uncertainty range of ~34%, of which ~15 to 18% is attributed to differences in codes/data and ~15% is attributed to differences in measuring techniques. If only the U.S. data are considered, the extreme uncertainties vary from 5 to 24%, of which ~12% is attributed to differences in codes and ~12% is attributed to differences in measuring techniques.

V.B. BEO Experiment

The edge-on arrangement of beryllium and Li_2O layers in a horizontally alternating pattern resulted in a substantial increase in the local TPR throughout the mixing zone. The preanalysis indicated an increase of ~30% in the global tritium breeding ratio (TBR) in comparison to the case where no Be is introduced in the assembly.[20,21,24] Local TPR from T_6 in the mixed zone (of 30-cm depth) increased by a factor of 3 as compared to the non-Be case, i.e., the reference experiment in phase IIA (Refs. 6, 10, and 11). This increase resulted from the enhancement in the neutron population in the adjacent Be layers through the Be(n,2n) reactions and to the moderation of neutrons by the elastic scattering processes in the Be layers. The T_7 also increased in the mixed region by ~8% but local values decreased thereafter by ~10%.

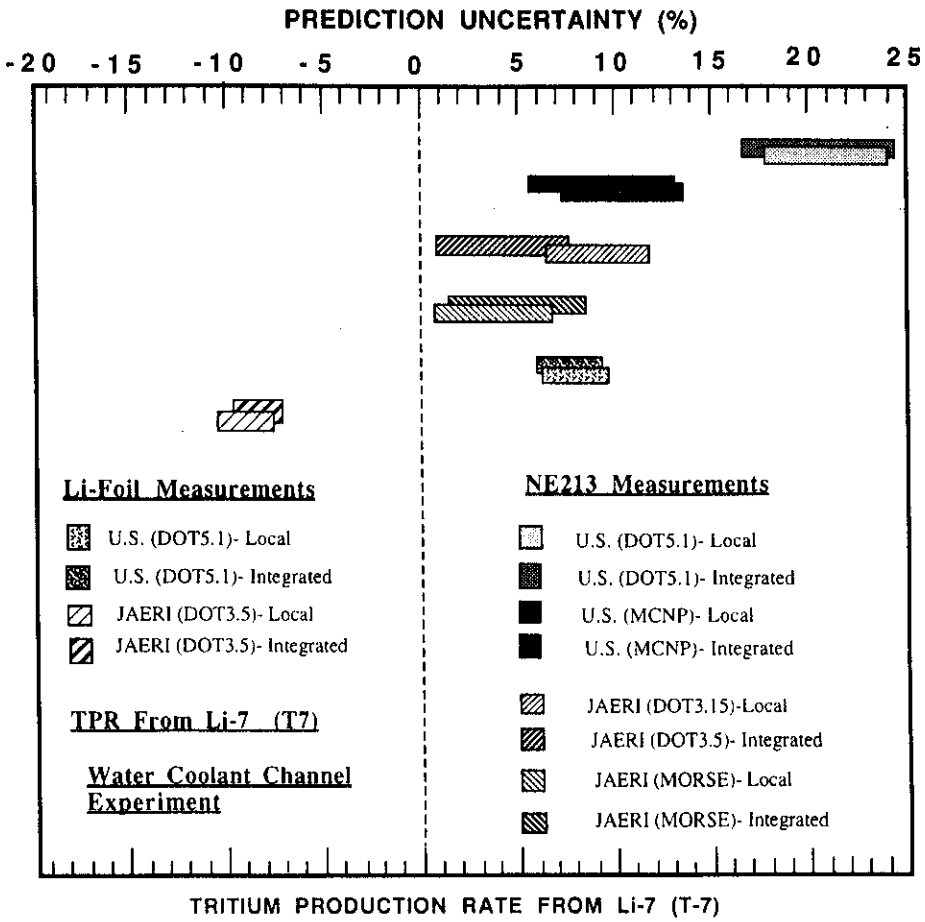

Fig. 12. The prediction uncertainties in local and integrated TPR from Li-7 in the WCC experiment.

V.B.1. Prediction Uncertainty of TPR from Li-6 and Nonthreshold Reactions

The (c/e)i values for T_6 measured by the Li-glass detectors are shown in Fig. 13 (numerical values are given in Table X). In comparison to Fig. 5, the values are more or less steady along the central axis with no abrupt change in shape. The values obtained by the U.S. are generally larger [$(c/e)_i$ ~0.85 to 1.05] than those obtained by JAERI [$(c/e)_i$ ~0.9 to 1.02]. In comparison to the no Be case (reference case in phase IIA experiments, see Refs. 10 and 11), the $(c/e)_i$ values are generally lower than unity by ~5 to 10%; while in the no Be case, the (c/e)i values are generally larger than unity by ~7 to 10%. This could be again related to the beryllium data and/or to the flux perturbation caused by the finite size of the Li-glass detectors used to measure T_6. In this regard, one should carefully evaluate the experimental data obtained by the Li-glass detectors. There is a large variation in T_6 profile along the vertical direction within the Be/Li_2O mixed zone, and also there are effects due to the presence of void behind the Li-glass detectors. For the former effect, it was shown that the zonal plate data of natural lithium at the mid-position are lower by ~15 to 17% than the average data over the 5-cm cell layer (see Ref. 19). On the other hand, the analysis has shown that the presence of the void amounts to higher T_6 values by ~20% at the center of the detectors. Thus, the Li-glass data are likely to be close to the average values over the 5-cm cell layer.

In calculating the $^{197}Au(n,\gamma)^{198}Au$ reaction rate along the central axis by the Monte Carlo method, large statistical errors were encountered, particularly in the MCNP calculations. The $(c/e)_i$ values for this reaction are shown in Fig. 14 where in the U.S. calculations these values are within ±40%. The reaction is also overestimated in JAERI's calculation by as much as 40% at the front locations. The overestimation is apparent in JAERI's calculations inside the beryllium heterogeneous region (up to a depth of 30 cm) and could be due to the way the calculations were performed with the Monte Carlo method. Track length estimations were considered for cells of ~5 cm diameter. Therefore, the

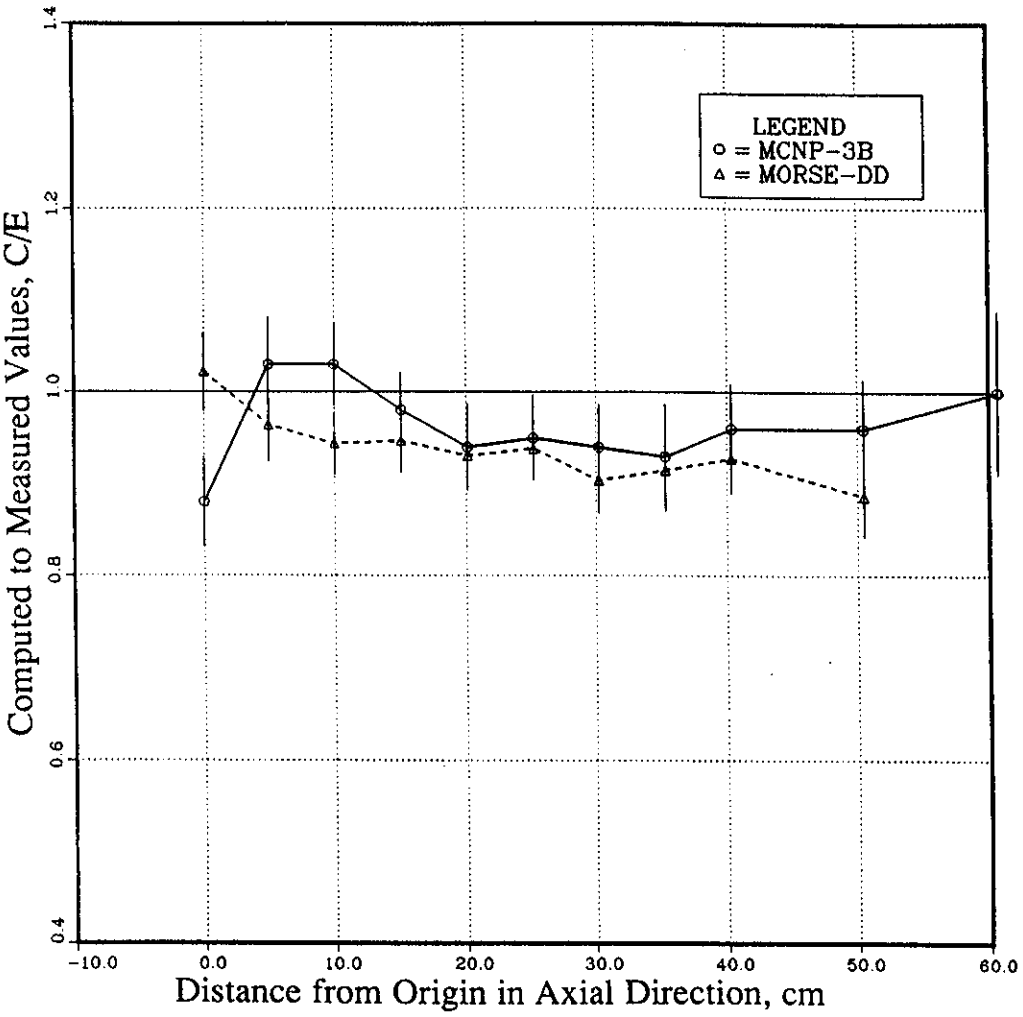

Fig. 13. The $(c/e)_i$ values of TPR from Li-6 (T_6) measured by Li-glass detectors along the central axis (BEO experiment).

estimates are the average values within these cells whereas the low-energy component of the flux is depressed at the center axis of the Li_2O zone where measurements were performed. A comparison of JAERI's results to those obtained in Phases IIA and IIB is shown in Fig. 15 where the $(c/e)_i$ values in these two phases are lower than unity at all locations. Note that in the Phase IIA and IIB experiments, no heterogeneity was introduced as in the Phase IIC BEO experiment.

V.B.2. Prediction Uncertainty of TPR from Li-7

In comparison to the corresponding values in the WCC experiment, (See Fig. 10), the $(c/e)_i$ values shown in Fig. 16 have a decreasing trend as one moves to the back locations (measurements performed by NE213 detectors). The local prediction accuracy in this case is within +10 and −15% and the U.S. values are on the average, larger than those obtained by JAERI by ~10%, although there is overlapping among the statistical errors in the Monte Carlo calculations at all locations. The numerical values of the experimental and calculational data are given in Table X. Figure 17 shows the comparison of the (c/e)i values obtained by JAERI with the MORSE-DD in the BEO experiment relative to the corresponding values obtained in the reference experiments of Phase IIA and Phase IIB (Refs. 10 and 11). The $(c/e)_i$ values in the BEO experiment are very similar to the ones obtained in the Phase IIB experiment and the descending trend is common in the three experiments. The agreement with measurements is better at the front location (within 5%), but the deviation from measurements increases at deeper locations.

V.B.3. Zonal TPR

As mentioned earlier, the TPRs were also measured in predesignated zones along the central and off-central

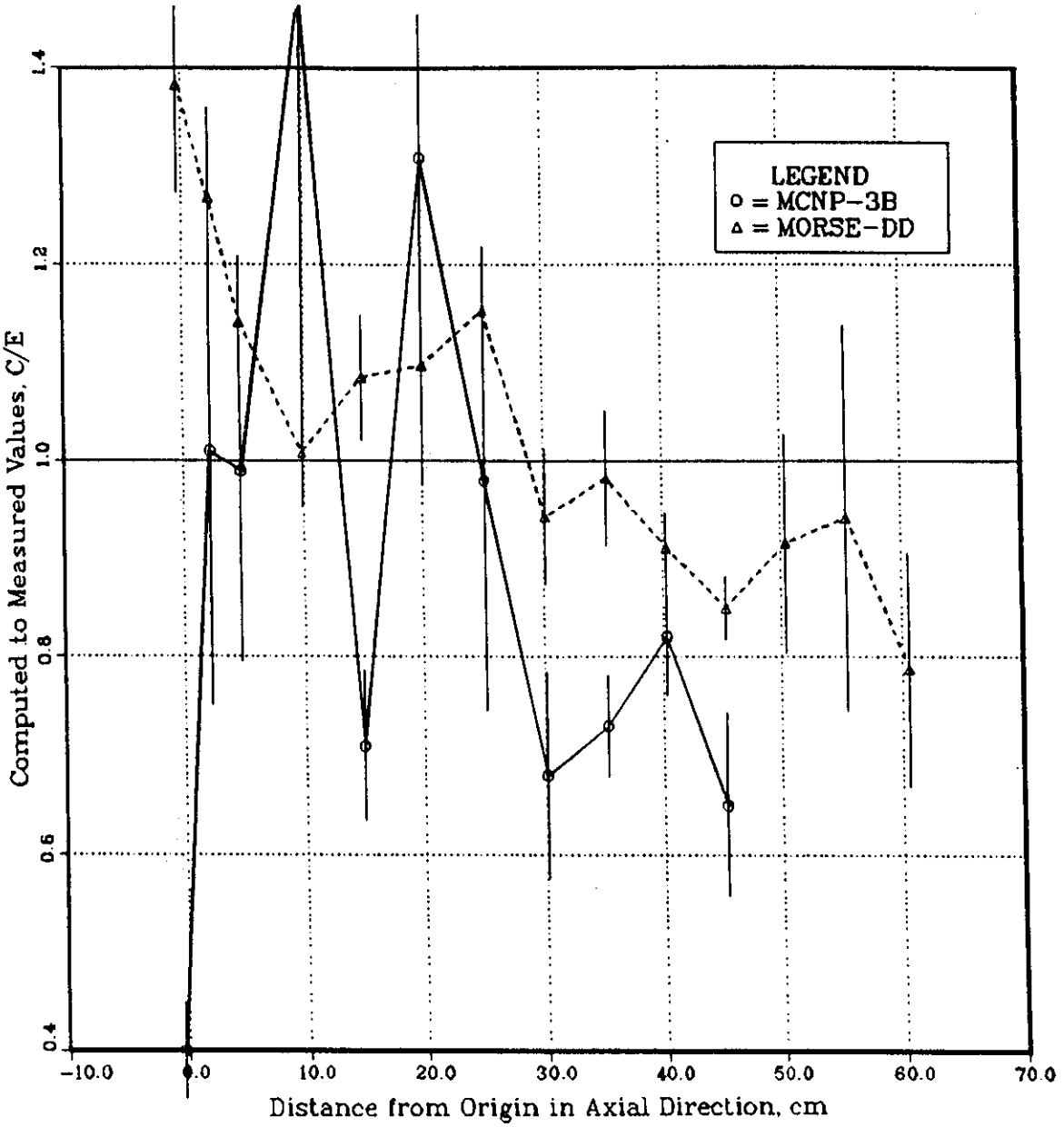

Fig. 14. The $(c/e)_i$ values of the Au-197(n,γ)Au-198 reaction rate along the central axis in the BEO experiment.

drawers (each has the dimensions of ~5.06 cm × ~5.06 cm × ~60 cm) using samples of natural lithium (Li-n) and ^{7}Li-enriched samples. The arrangement of the zonal samples can be found in Refs. 20 and 21. Figure 18 shows the $(c/e)_i$ values of tritium production rate from natural lithium, Li-n (T_n), along the central drawer. The $(c/e)_i$ values are within ± 5% up to a distance of 45 cm. Thereafter, the $(c/e)_i$ values are larger than unity by ~10 to 25% in the MCNP calculations (the statistical errors in the back zones are as large as 10%). The $(c/e)_i$ values for T_7 measured by this zonal technique are lower than unity in all zones by as much as ~15%, as shown in Fig. 19, except in the last zone where the underestimation in T_7 is ~40%. Table XI gives the numerical $(c/e)_j$ values for T_7 and T_n along with the associated relative standard deviation at each zone j.

V.B.4. Prediction Uncertainties of Local and Integrated TPR

The fitting curves for the experimental data of T_6 measured by Li-glass detectors and the calculational data, along with their associated absolute standard deviations, are shown in Fig 20. The features of the curves

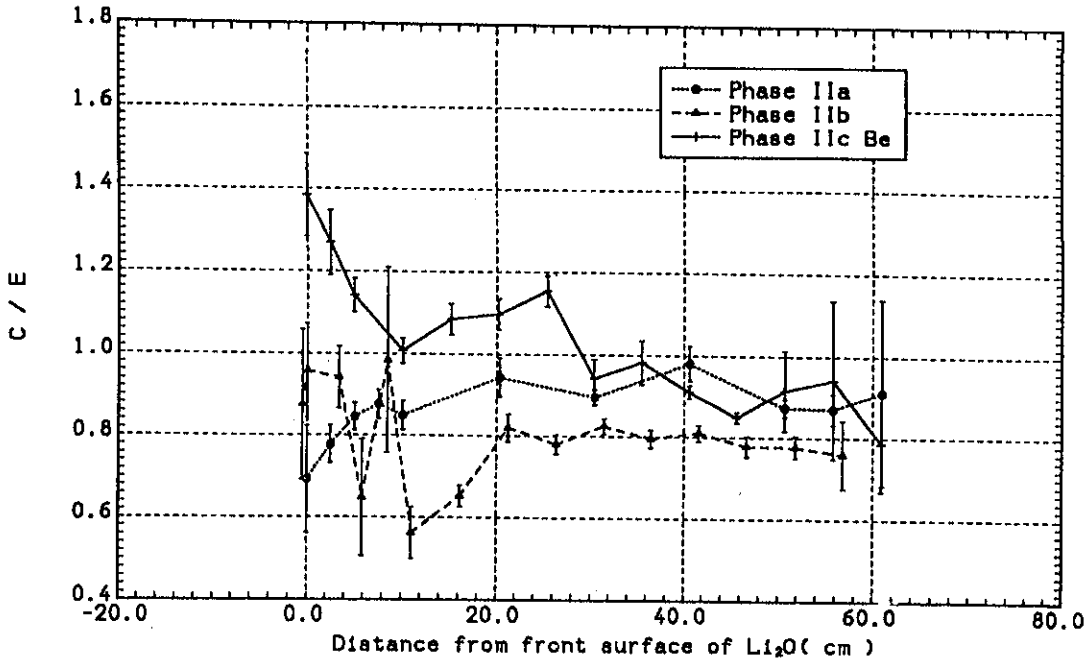

Fig. 15. The $(c/e)_i$ values of the Au-197(n,γ)Au-198 reaction rate along the central axis in Phases IIA, IIB, and IIC (BEO) experiments.

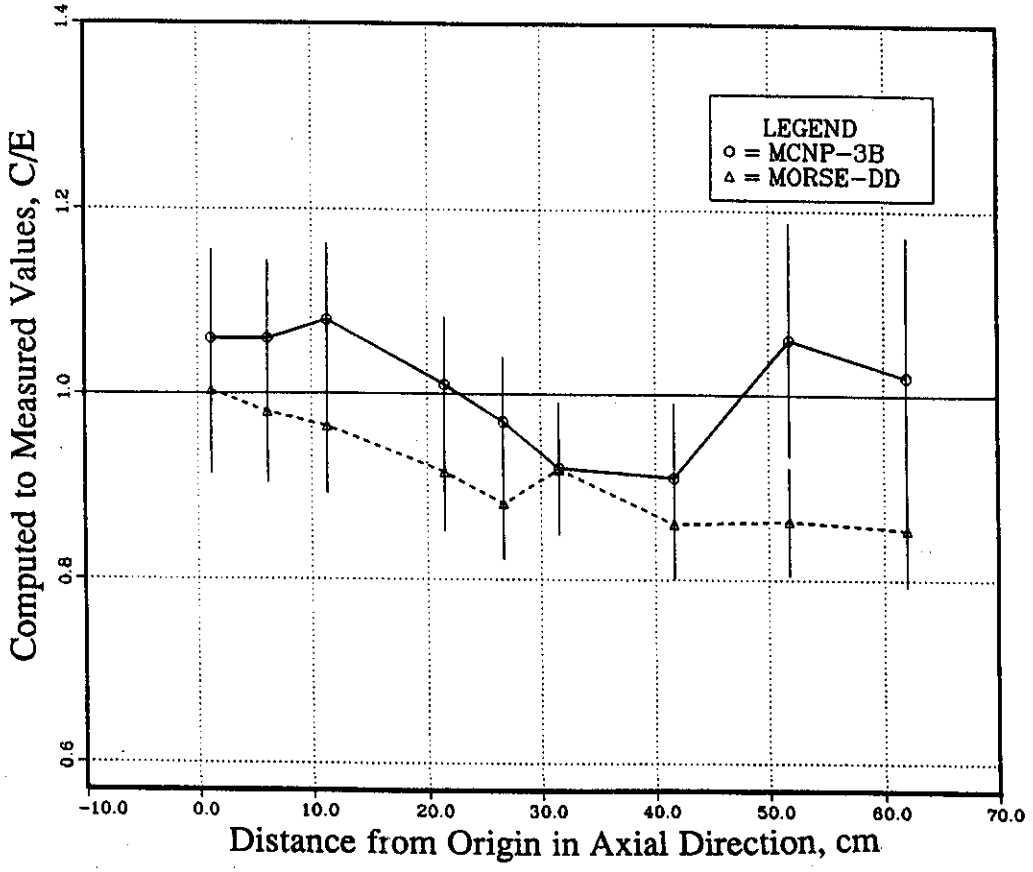

Fig. 16. The $(c/e)_i$ values of TPR from Li-7 (T_7) measured by NE213 detectors along the central axis (BEO experiment).

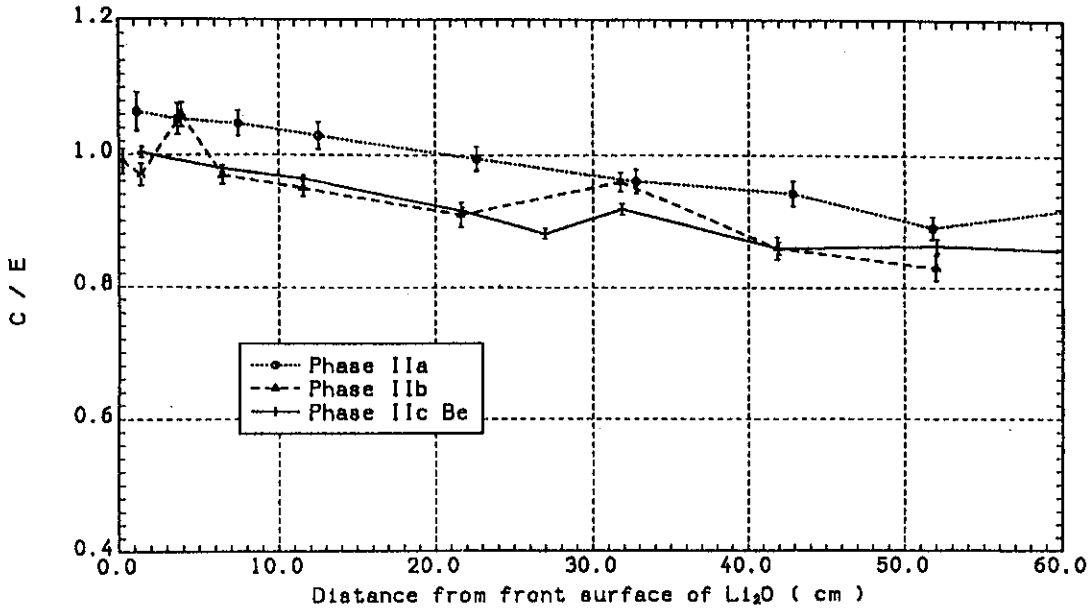

Fig. 17. The $(c/e)_i$ values of TPR from Li-7 (T_7) measured by NE213 detectors along the central axis in Phases IIA, IIB, and IIC (BEO) experiments.

TABLE X

Calculated and Experimental Data of TPR from Li-6 and Li-7 Along the Central Axis of the BEO Experiment

No.	Depth (cm)	Experimental Value, e	Calculated Value, c (U.S.)	c/e (U.S.)	Calculated Value, c (JAERI)	c/e (JAERI)
TPR from Li-6 (Li-Glass Measurements)						
1	−0.1	1.85−28[a] (4.1[b])	1.63−28 (3.8[c])	0.88 (5.6)	1.89−28 (1.3)	1.02 (4.9)
2	4.93	2.36−28 (4.1)	2.43−28 (3.0)	1.03 (5.1)	2.27−29 (1.1)	0.96 (4.2)
3	9.99	2.49−28 (3.5)	2.56−28 (2.7)	1.03 (4.4)	2.35−28 (1.0)	0.94 (3.6)
4	15.05	2.27−28 (3.5)	2.23−28 (2.3)	0.98 (4.2)	2.15−28 (1.1)	0.95 (3.7)
5	20.11	1.89−28 (3.4)	1.78−28 (3.4)	0.94 (4.8)	1.76−28 (1.1)	0.93 (3.6)
6	25.17	1.31−28 (3.4)	1.24−28 (3.4)	0.95 (4.8)	1.23−28 (1.1)	0.94 (3.6)
7	30.23	6.78−29 (3.2)	6.37−29 (3.2)	0.94 (4.5)	6.13−29 (1.3)	0.90 (3.5)
8	35.29	3.40−29 (3.8)	3.16−29 (3.8)	0.93 (5.4)	3.11−29 (1.2)	0.91 (4.0)
9	40.35	2.14−29 (3.3)	2.06−29 (3.3)	0.96 (4.7)	1.99−29 (1.2)	0.93 (3.5)
10	50.47	1.12−29 (3.0)	1.08−29 (3.0)	0.96 (4.2)	9.95−30 (1.6)	0.88 (3.4)
TPR from Li-7 (NE312 Measurements)						
1	1.2	5.48−30 (9.0)	5.81−30 (1.3)	1.06 (9.1)	5.50−30 (0.8)	1.00 (9.0)
2	6.2	4.34−30 (7.8)	4.59−30 (1.8)	1.06 (8.0)	4.25−30 (0.7)	0.98 (7.8)
3	11.3	3.13−30 (7.5)	3.38−30 (1.7)	1.08 (7.7)	3.02−30 (0.6)	0.96 (7.5)
4	21.5	1.43−30 (6.9)	1.44−30 (2.4)	1.01 (7.3)	1.31−30 (0.8)	0.92 (6.9)
5	26.7	9.17−31 (6.8)	8.89−31 (2.7)	0.97 (7.3)	8.09−31 (1.0)	0.88 (6.9)
6	31.6	5.75−31 (6.8)	5.29−31 (3.8)	0.92 (7.8)	5.28−31 (1.2)	0.92 (6.9)
7	41.7	2.51−31 (6.8)	2.28−31 (5.7)	0.91 (8.9)	2.16−31 (1.4)	0.86 (6.9)
8	51.8	1.04−31 (6.6)	1.11−31 (10.0)	1.07 (11.9)	9.02−32 (1.7)	0.88 (6.8)

Note: Units in (T atom/Li atom/source neutron).
[a]Read as 1.85×10^{-28}.
[b]Relative standard deviation in measurements (%).
[c]Relative standard deviation in calculations (%).

TABLE XI

Calculated and Experimental Data for Zonal TPR from Li-7 (T_7) and from Natural Lithium Along the Central Axis of the BEO Experiment

Distance of Boundaries from Front Edge (cm)	Thickness (cm)	Experimental Value, e	Calculated Value, c (U.S.)	c/e (U.S.)	Calculated Value, c (JAERI)	c/e (JAERI)
Zonal TPR from Natural Lithium (Tn)						
0.0 to 5.1	5.1	2.04−29[a] (2.9[b])	2.02−29 (2.6[c])	0.99 (3.9)	2.08−29[c]	1.02
5.1 to 9.9	4.8	2.21−29 (3.2)	2.28−29 (2.7)	1.03 (4.2)	2.12−29	0.96
9.9 to 14.9	5.0	2.03−29 (3.0)	2.07−29 (2.7)	1.02 (4.0)	1.93−29	0.95
14.9 to 20.0	5.1	1.67−29 (3.0)	1.75−29 (2.6)	1.05 (3.9)	1.63−29	0.97
20.0 to 24.96	4.96	1.33−29 (3.0)	1.29−29 (2.5)	0.97 (3.9)	1.24−29	0.9
24.96 to 29.76	4.8	8.31−30 (3.0)	7.89−30 (2.2)	0.95 (3.7)	7.77−30	0.94
30.2 to 35.22	5.02	3.67−30 (3.0)	3.52−30 (3.0)	0.96 (4.2)	3.41−30	0.93
35.22 to 40.32	5.1	2.01−30 (3.0)	2.23−30 (4.9)	1.11 (5.7)	2.04−30	1.01
40.32 to 45.42	5.1	1.30−30 (3.1)	1.39−30 (8.8)	1.07 (9.3)	1.36−30	1.05
45.42 to 50.22	4.8	1.03−30 (2.9)	1.25−30 (10.1)	1.22 (10.2)	9.62−31	0.94
Zonal TPR from Li-7						
0.0 to 5.1	5.1	5.51−30 (3.1)	5.45−30 (1.0)	0.99 (3.3)	5.23−30	0.95
9.9 to 14.9	5.0	3.23−30 (3.1)	2.87−30 (2.7)	0.89 (4.1)	2.82−30	0.88
20.0 to 24.96	4.96	1.47−30 (2.7)	1.27−30 (3.7)	0.86 (4.6)	1.23−30	0.84
30.2 to 35.22	5.02	5.56−31 (3.1)	5.45−31 (5.9)	0.98 (6.7)	4.90−31	0.81
45.42	4.8	1.98−31 (3.0)	1.23−31 (13.8)	0.62 (14.1)	1.29−31	0.65

Note: Units in (T atom/Li atom/source neutron).
[a]Read as 2.04×10^{-29}.
[b]Relative standard deviation in measurements (%).
[c]Relative standard deviation in calculations (%).

are consistent with the $(c/e)_i$ values shown in Fig. 13, i.e., overestimation in the U.S. results at the second and third locations while underestimation in JAERI's results at all locations, except the first. In deriving the fitting curves, two subzones were considered with boundaries of z = 0 to 20 cm and z = 20 to 51 cm. Quadrature fitting curves (of second degree) were considered for the first five locations. The data at the last six locations were also fitted with second-degree polynomials. As shown, local T_6 increases up to a depth of ~10 cm; then its profile starts to drop thereafter. The fitting curves for local T_7 measured by NE213 detectors are shown in Fig. 21, and their shapes are consistent with the results shown in Fig. 16. Polynomials of the third degree were considered in this case where all the eight data points shown in Table X were accounted for in one zone.

The prediction uncertainties and the associated relative standard deviations in the average local and integrated T_6 and T_7 measured by Li-glass and NE213 detectors are shown in Table XII. The corresponding values for T_7 and T_n measured by zonal method are also shown. The prediction uncertainties and standard deviations in the latter case are calculated using Eqs. (15), (16), and (17). In addition, the uncertainties in the local TPR from natural lithium and the associated standard deviations were calculated from the calculational and the combined experimental data of the Li-glass and NE213 measurements according to Eqs. (18) through (21). The corresponding values for the integrated T_n were also calculated according to Eqs. (22) through (25) and are introduced in Table XII. Table XIII gives the required parameters needed to apply Eqs. (22) through (25) based on the U.S. and JAERI's results. It is worth noting that in order to combine the calculational and experimental data of TPR from Li-6 and Li-7 according to Eq. (18), it was necessary to use the fitting curves shown in Figs. 20 and 21 since the locations of the T_6 and T_7 measurements are not the same. Using the fitting curves also enabled us to calculate the $(c/e)_i$ values for T_n and the associated variances at practically any location on the central axis. These smooth $(c/e)_i$ curves are shown in Fig. 18 and are labeled (T6+T7) and a comparison to the values obtained directly from the zonal measurements could be made. Figure 22 shows these curves where the combined errors (variances) of the calculational and experimental data are accounted for at each location, leading to distinct boundaries of envelopes

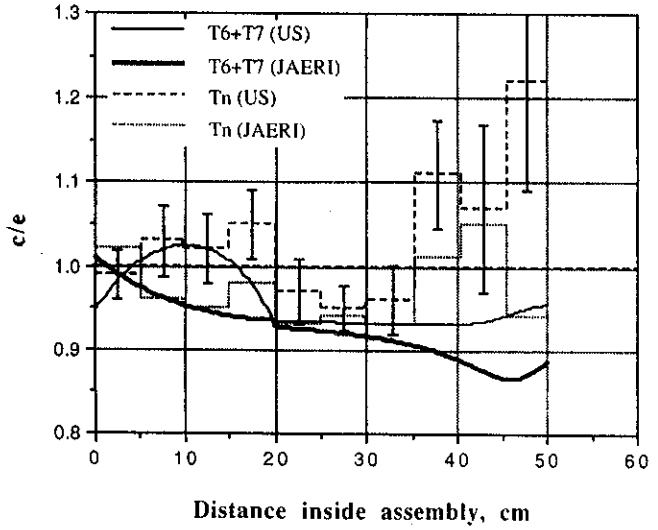

Fig. 18. The $(c/e)_i$ values of zonal TPR from natural lithium (T_n) along the central axis (BEO experiment).

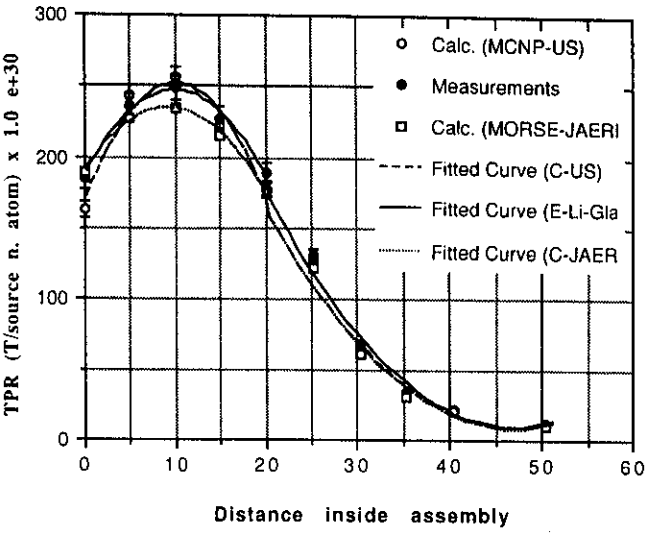

Fig. 20. Calculational and experimental data sets and the fitting curves for T_6 measured by Li-glass detectors in the BEO experiment.

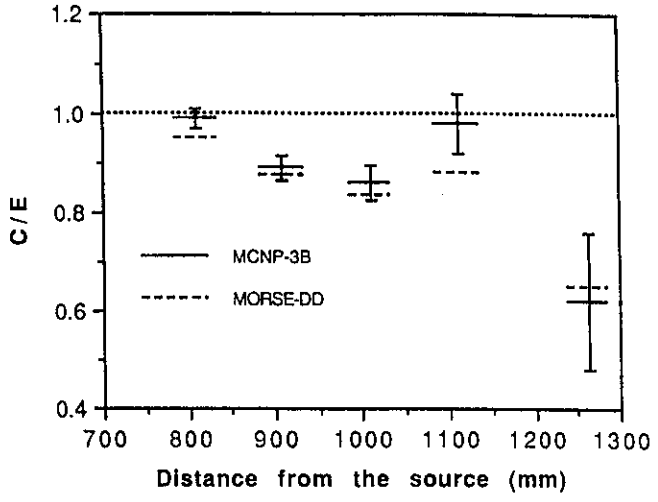

Fig. 19. The $(c/e)_i$ values of TPR from Li-7 (T_7) obtained from zonal TPR measurements in the BEO experiment.

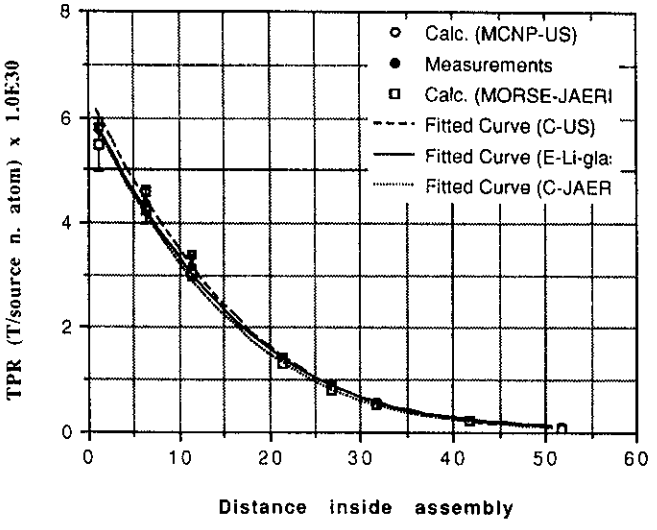

Fig. 21. Calculational and experimental data sets and the fitting curves for T_7 measured by NE213 detectors in the BEO experiment.

that are apart by 5 to 18%, with larger uncertainties occurring toward back locations. Figure 23 gives the graphical form of the data presented in Table XII. From these tables and figures we notice that the average local C/E values for T_6, T_7, and T_n are lower than those corresponding to the integrated values. In addition, the relative standard deviations, σ_{Ir}, seem to be larger for the C/E of the integrated TPR than those of the C/E of local TPR. These deviations are in the order of 1.3 to 3.6%. The following can also be observed:

T_6:

1. Both local and integrated values for T_6 are underpredicted. The integrated values are underpredicted by about *−2.8% (U.S.) and −5.5% (JAERI)*. The calculated values obtained by the U.S. are larger by ~3% than those obtained by JAERI. This difference, however, is within $\pm\sigma$ and is smaller than the corresponding difference found in the Monte Carlo results of the WCC experiment.

TABLE XII

The Prediction Uncertainties (%) in Local and Integrated TPR of the BEO Experiment

Items	U.S. MCNP	JAERI MORSE-DD
T_6		
Li-glass		
Local	−3.9[a] (1.6[b])	−7.2 (1.3)
Integrated	−2.8 (1.8)	−5.5 (1.5)
T_7		
NE213		
Local	−0.3 (2.9)	−8.2 (2.5)
Integrated	3.1 (3.6)	−4.0 (3.5)
Zonal		
Local	−9.4 (2.2)	−11.5 (2.0)
Integrated	−6.4 (2.3)	−8.9 (2.3)
Tn		
Zonal		
Local	0.42 (1.6)	−5.0 (1.3)
Integrated	1.5 (1.6)	−3.3 (1.6)
Combined		
Local	−5.3 (2.4)	−7.2 (2.1)
Integrated	−2.0 (1.6)	−5.0 (1.3)

[a]Prediction uncertainty [(C/E) − 1] × 100.
[b]Relative standard deviation, σ_r (%).

2. Considering only the integrated TPR, its extreme uncertainties (accounting for σ's) in T_6 prediction vary from about −7 to −1%, reflecting the differences due to code/data used by the U.S. and JAERI. If only the U.S. results are considered, these extreme uncertainties are −4.5 to −1%.

T_7:

1. Based on NE213 measurements, the average local TPR is underpredicted in both the U.S. (−0.3%) and JAERI's (−8.2%) calculations. The integrated TPR is over predicted by *~3% in the U.S. calculations while underpredicted by about −4%* in JAERI's calculation. The U.S. calculations are larger than JAERI's by ~7%, which is less than in the case of WCC experiment (15 to 18%).

2. The prediction uncertainties in both local and integrated TPR have larger deviations (2 to 3.6%) than the ones found for T_6 (1.3 to 1.8%). This is due to the larger experimental uncertainties in NE213 measurements than the uncertainties in Li-glass measurements (see Table X).

3. With Zonal measurements, larger underestimation is observed in both local and integrated values. The prediction uncertainties in the integrated TPR are about *−6% (U.S.) and about −9% (JAERI).*

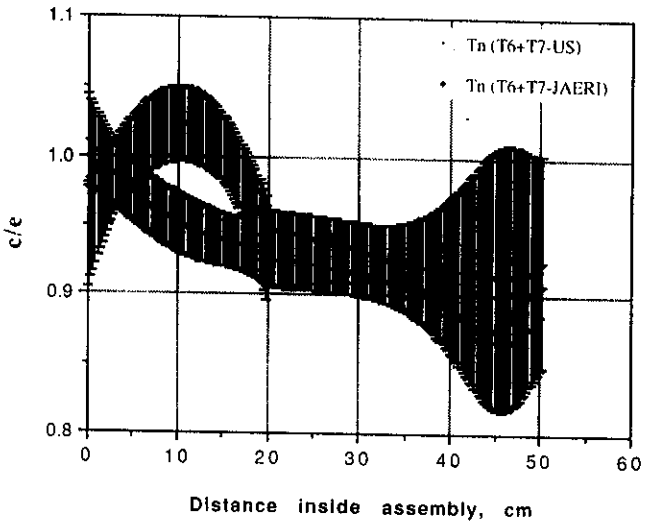

Fig. 22. The envelopes of the uncertainty in the $(c/e)_i$ values of TPR from natural lithium obtained from T_6 and T_7 measurements by Li-glass and NE213 detectors.

TABLE XIII

Integrated Parameters Required to Estimate the Prediction Uncertainty in the Integrated TPR from Natural Lithium Based on Li-Glass and NE213 Experimental Data in the BEO Experiment

	TPR from Li-6			TPR from Li-7	
Parameter	U.S.	JAERI	Parameter	U.S.	JAERI
C_6	6171[a]	6002	C_7	90	84
σ_{C6}	67[b]	24	σ_{C7}	0.7	0.3
E6	6348	6348	E_7	88	88
σ_{E6}	89	89	σ_{E7}	3.1	3.1

[a]Units: [T atom·cm/Li-atom/source neutron] × 10^{30}.
[b]Absolute standard deviation.

4. Considering only the integrated TPR from both the NE213 and zonal measurements, its extreme uncertainties in T_7 vary from about −11 to 7% (an uncertainty range of ~18%), of which 5 to 9% is attributed to differences in measuring techniques. If only the U.S. results are considered, these extreme uncertainties vary from about −9 to ~7%, of which ~9% is attributed to differences in measuring techniques.

T_n:

1. The prediction uncertainties in integrated T_n obtained from zonal measurements are estimated as *~1.5% (U.S.) and −3.3% (JAERI) with relative standard deviation of ~1.6%*. These uncertainties are lower than those associated with the integrated T_6 and T_7.

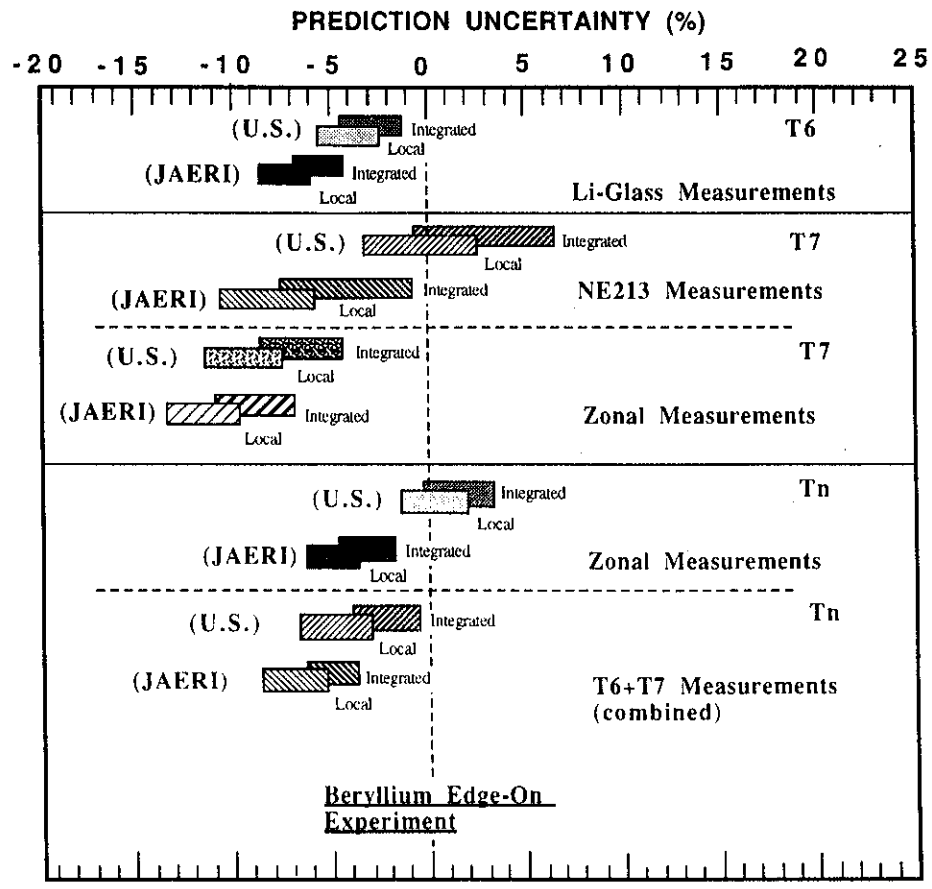

Fig. 23. The prediction uncertainties in local and integrated TPR from Li-6, Li-7, and natural lithium in the BEO experiment.

2. When T_n is estimated from the calculational and experimental data of the integrated T_6 and T_7, the prediction uncertainties become slightly larger (−2%, U.S.; −5%, JAERI) indicating that the combined experimental databases on NE213 and Li-glass measurements are larger than zonal measurements by ~2 to 3.5%. Since T_n is dominated by contribution from T_6 values, the uncertainty in the integrated T_n and its associated relative deviation are similar to those of T_6.

3. Considering the integrated T_n obtained by both techniques, the extreme uncertainties vary from −6 to 3% with ~2 to 4% attributed to differences in measuring techniques. If only the U.S. results are considered, these uncertainties vary from −3.6 to 3%, with ~3.5% attributed to differences in experimental techniques.

VI. SUMMARY

The WCC and the BEO experiments were specifically chosen for Phase IIC in order to examine the prediction capabilities for tritium production, in-system spectra, and other reaction rates in systems that are characterized by design heterogeneities found in various blanket designs. Comparisons were made to measurements and to results from previous phases of experiments. In general, it was found that, even with system heterogeneities, the present codes and data libraries can reasonably predict these neutronics parameters with no specific difficulties.

The prediction accuracy for T_7 in the WCC system is within ±15% in JAERI calculations, but larger divergences were found in the U.S. calculations [$(c/e)_i$ ~1.1 to 1.25] based on the NE213 measurements. Closer values to unity were observed in the BEO system [$(c/e)_i$ ~0.9 to 1.1]. The results obtained by the Li-foil measurements give, on the average, closer $(c/e)_i$ values to unity than those obtained by the NE213 method. When the zonal method was applied, it was found that the $(c/e)_i$ values were lower than unity by ~5 to 15% while TPR from natural lithium (T_n) is ±5 to 10% up to a depth of 45 cm in the BEO system.

Unlike the threshold reaction, T_6 and $^{197}Au(n,\gamma)$ reactions exhibit steep profiles around the coolant channels in the WCC system. The $(c/e)_i$ curves for T_6 and $^{197}Au(n,\gamma)$ are not as flat as those for the high-threshold reactions when heterogeneities are crossed

and gradients occur near them. The divergence in the calculations for T_6 around heterogeneities is about ±20 to 25% (Li-glass detectors) and is ±25 to 30% for $^{197}Au(n,\gamma)$ in the WCC system. With Li-foil detectors, the $(c/e)_i$ values were lessened by ~5 to 10%. In the BEO, the $(c/e)_i$ were less than unity (Li-glass detectors). This could be related to the beryllium data since it was observed, as in the case in the other phases, that predictions are lower than measurements near Be/Li_2O boundaries. The discrepancy could also be attributed to the geometrical effects of the Li-glass detector itself when used to measure T_6.

The prediction uncertainties in local and line-integrated TPR, and the associated standard deviations, were also performed in the two systems by applying a statistical approach in which the calculational and experimental errors at each measuring point were accounted for. These are meaningful quantities for designers who are interested in knowing the current uncertainties in T_6, T_7, and T_n in similar systems for proper safety factors assignment. This study revealed the following:

1. In the WCC experiment, the uncertainty in the integrated T_6 could fall anywhere between −13 and 21%. Out of this uncertainty range (of ~34%), 10 to 15% is attributed to differences in codes/data used by the U.S. and JAERI and 10 to 18% is attributed to differences in measuring techniques (Li-glass and Li-foil measurements). In the BEO experiment, the prediction uncertainties were estimated to vary between −7 and −1% (lesser values than those found in the WCC experiment). This range reflects the differences between the codes/data used by the U.S. and JAERI and the experimental errors of data taken by Li-glass detectors.

2. The integrated T_7 in the WCC experiment showed uncertainties that could be in between −10 to 24% (~34% uncertainty range). About 15 to 18% of this uncertainty range could be attributed to differences in codes/data and ~15% to differences between measuring techniques. The range of uncertainties estimated in the BEO experiment is ~18% (from −11 to 7%); about 5 to 9% of this range is caused by the differences found between zonal measurements and NE213 measurements.

3. The window of uncertainties in the prediction of TPR from natural lithium (T_n) was estimated in the BEO experiment to be ~9% (uncertainties range from −6 to ~3%) of which ~2 to 4% was attributed to differences between zonal measurements and the combined experimental data of T_6 (measured by Li-glass detectors) and T_7 (measured by NE213 detectors).

It is worth noting that the differences between various techniques to measure the tritium production rate are still large, and in some cases (as in T_6 measurements in the WCC experiment) larger than the margins in TBR calculations considered by blanket designers. This is a serious situation that requires further benchmarking and measuring techniques evaluation and/or development. An effort in this direction was recently pursued in an international comparison on measuring techniques of tritium production rate. It was found that, even using same technique, i.e., Dierckx' liquid scintillation technique, to measure tritium production rate, a disagreement of more than 10% was seen among different participants even though the expected accuracy was 3 to 5% (Ref. 39).

ACKNOWLEDGMENT

The U.S. contribution to the joint collaborative program is supported by the U.S. Department of Energy, Office of Fusion Energy, under contract DE-FG03-86ER52123.

REFERENCES

1. T. NAKAMURA and M. A. ABDOU, "Summary of Recent Results from the JAERI/U.S. Fusion Neutronics Phase I Experiments," *Fusion Technol.*, **10**, 541 (1986).

2. M. Z. YOUSSEF et al., "Analysis and Inter Comparison for Phase I Fusion Integral Experiments at the FNS Facility," *Fusion Technol.*, **10**, 549 (1986).

3. M. Z. YOUSSEF et al., "Phase I Fusion Integral Experiments, Vol. II: Analysis," UCLA-ENG-88-15, University of California, Los Angeles (Sep. 1988); see also JAERI-M-88-177, Japan Atomic Energy Research Institute (Aug. 1988).

4. M. NAKAGAWA et al., "Analysis of Neutronics Parameters Measured in Phase II Experiments of JAERI/U.S. Collaborative Program on Breeder Neutronics, Part I: Source Characteristics and Reaction Rate Distribution," *Fusion Eng. Des.*, **9**, 315 (1989).

5. Y. OYAMA et al., "Phase II Experimental Results of JAERI/USDOE Collaborative Program on Fusion Blanket Neutronics Experiments," *Fusion Eng. Des.*, **9**, 309 (1989).

6. M. Z. YOUSSEF et al., "Analysis of Neutronics Parameters Measured in Phase II Experiments of the JAERI/U.S. Collaborative Program on Fusion Blanket Neutronics, Part II: Tritium Production and In-System Spectrum," *Fusion Eng. Des.*, **9**, 323 (1989).

7. Y. OYAMA et al., "Phase IIB Experiments of JAERI/USDOE Collaborative Program on Fusion Blanket Neutronics," *Fusion Technol.*, **15**, 1293 (1989).

8. M. Z. YOUSSEF et al., "Comparative Analysis for Phase IIA and IIB Experiments of the U.S./JAERI Collaborative Program on Fusion Blanket Neutronics," *Fusion Technol.*, **15**, 1299 (1989).

9. Y. IKEDA et al., "Determination of Neutron Spectrum in D-T Fusion Field by Foil Activation Technique," *Fusion Technol.*, **15**, 1287 (1989).

10. M. Z. YOUSSEF et al., "The U.S./JAERI Collaborative Program on Fusion Neutronics; Phase IIA and IIB Fusion Integral Experiments, The U.S. Analysis," UCLA-ENG-90-14, University of California, Los Angeles (Dec. 1989).

11. M. NAKAGAWA et al., "JAERI/U.S. Collaborative Program on Fusion Blanket Neutronics, Analysis of Phase IIA and IIB Experiments," JAERI-M-89-154, Japan Atomic Energy Research Institute (Oct. 1989).

12. M. NAKAGAWA and T. MORI, "Reactor Engineering Department Annual Report—April 1, 1988 to March 31, 1989," JAERI-M-98-128, p. 129, Japan Atomic Energy Research Institute (Sep. 1989).

13. M. Z. YOUSSEF et al., "The Nuclear Analysis of an Annular Li_2O Blanket System Surrounding an Artificially Simulated 14-MeV Line Source and Comparison of Calculations to Measurements," *Fusion Technol.*, **28**, 320 (1995).

14. Y. OYAMA et al., "Concept and Characteristics of a Simulated Line Source for Annular Blanket Experiments Using an Accelerator-Based Deuterium-Tritium Neutron Source," *Fusion Technol.*, **28**, 305 (1995).

15. M. Z. YOUSSEF et al., "Analysis for the Simulation of a Line Source by a 14 MeV Moving Point Source and Impact on Blanket Characteristics: The USDOE/JAERI Collaborative Program on Fusion Neutronics," *Fusion Technol.*, **19**, Part 2B, 1843 (1991).

16. T. NAKAMURA et al., "A Line D-T Neutron Source Facility for Annular Blanket Experiment: Phase III of the JAERI/USDOE Collaborative Program on Fusion Neutronics," *Fusion Technol.*, **19**, Part 2B, 1873 (1991).

17. Y. OYAMA et al., "Annular Blanket Experiment Using a Line DT Neutron Source: Phase IIIA of the JAERI/USDOE Collaborative Program on Fusion Neutronics," *Fusion Technol.*, **19**, Part 2B, 1879 (1991).

18. C. KONNO et al., "Measurements of the Source Term for Annular Blanket Experiment with a Line Source: Phase IIIA of the JAERI/USDOE Collaborative Program on Fusion Neutronics," *Fusion Technol.*, **19**, Part 2B, 1885 (1991).

19. Y. OYAMA et al., "Neutronics Integral Experiments of Lithium-Oxide Fusion Blanket with Heterogeneous Configuration Using Deuterium-Tritium Neutrons," *Fusion Technol.*, **28**, 216 (1995).

20. Y. OYAMA et al.,"Phase-IIC Experiments of the USDOE/JAERI Collaborative Program on Fusion Blanket Neutronics—Experiments and Analysis of the Heterogeneous Fusion Blankets—Volume I: Experimental Results," JAERI-M-92-182, Japan Atomic Energy Research Institute (Dec. 1992); see also UCLA-FNT-63, UCLA-ENG-93-18, University of California, Los Angeles (Dec. 1992).

21. M. Z. YOUSSEF et al.,"Phase-IIC Experiments of the USDOE/JAERI Collaborative Program on Fusion Blanket Neutronics—Experiments and Analysis of the Heterogeneous Fusion Blankets—Volume II: Analysis," UCLA-FNT-64, UCLA-ENG-93-19, University of California, Los Angeles (Dec. 1992); see also M. NAKAGAWA et al., JAERI-M-92-183, Japan Atomic Energy Research Institute (Dec. 1992).

22. M. YOUSSEF et al., "Analysis for Heterogeneous Blankets and Comparison to Measurements: Phase IIC Experiments of the USDOE/JAERI Collaborative Program on Fusion Neutronics," *Fusion Technol.*, **19**, Part 2B, 1891 (1991).

23. Y. OYAMA et al., "Measured Characteristics of Be Multi-Layered and Coolant Channel Blankets: Phase IIC Experiments of the JAERI/USDOE Collaborative Program on Fusion Neutronics," *Fusion Technol.*, **19**, Part 2B, 1955 (1991).

24. A. KUMAR, Y. WATANABE, and M. YOUSSEF, "Analysis of the Selection of Experimental Configuration for Heterogeneity and Be Multi-Layered Experiments of the USDOE/JAERI Collaborative Program on Blanket Neutronics," *Fusion Technol.*, **15**, 1309 (1989).

25. LOS ALAMOS MONTE CARLO GROUP, "MCNP—A General Monte Carlo Code for Neutron and Photon Transport," Version 3A, LA-7396, Rev. 2, Los Alamos National Laboratory (1986).

26. M. NAKAGAWA and T. MORI, "MORSE—DD, A Monte Carlo Code Using Multigroup Double Differential Form Cross-Sections," JAERI-M84-126, Japan Atomic Energy Research Institute (July 1984).

27. L. P. KU and J. KOLIBAL, "RUFF—A Ray Tracing Program to Generate Uncollided Flux and First Collision Source Moments for DOT4, A User's Manual," EAD-R-16, Plasma Physics Laboratory, Princeton University (1985).

28. W. A. RHOADES and R. L. CHILDS, "An Updated Version of the DOT 4 (Version 4.3) One-and-Two-Dimensional Neutron/Photon Transport Code," ORNL-5851, Oak Ridge National Laboratory (Apr. 1982); see also CCC-429, Radiation Shielding Information Center (1982).

29. "DOT 3.5: Two-Dimensional Discrete Ordinates Radiation Transport Code," CCC-276, Radiation Shielding Information Center; see also W. A. RHOADES and F. R. MYNETT, "The DOT III Two-Dimensional Discrete Ordinates Transport Code," ORNL-TM-4280, Oak Ridge National Laboratory (Sep. 1973).

30. R. A. MacFARLANE, "TRANSX-CTR: A Code for Interfacing MATXS Cross-Section Libraries to Nuclear Transport Codes for Fusion Systems Analysis," LA-9863-MS, Los Alamos National Laboratory (Feb. 1984).

31. M. Z. YOUSSEF et al., "The Prediction Capability for Tritium Production and Other Reaction Rates in Various Systems Configurations for a Series of the USDOE/JAERI Collaborative Fusion Blanket Experiments," *Fusion Eng. Des.*, **18**, 407 (1991).

32. M. Z. YOUSSEF et al., "Fusion Integral Experiments and Analysis and the Determination of Design Safety Factors—I: Methodology," *Fusion Technol.*, **28**, 366 (1995).

33. Y. IKEDA and M. Z. YOUSSEF, "Two-Dimensional Cross-Section Sensitivity and Uncertainty Analysis for Tritium Production Rate in Fusion-Oriented Integral Experiments," *Fusion Technol.*, **13**, 616 (1988).

34. P. M. SONG, M. Z. YOUSSEF, and M. A. ABDOU, "New Approach and Computational Algorithm for Sensitivity/Uncertainty Analysis for SED and SAD with Application to Beryllium Integral Experiments," *Nucl. Sci. Eng.*, **113**, 339 (1993).

35. M. Z. YOUSSEF and M. A. ABDOU, "Uncertainties in Prediction of Tritium Breeding in Candidate Blanket Designs Due to Present Uncertainties in Nuclear Data Base," *Fusion Technol.*, **9**, 286 (1986).

36. M. Z. YOUSSEF and Y. OYAMA, "Required Design Margins and Their Economic Impact in Fusion Reactors to Compensate for Nuclear Data Uncertainties—A Global Approach to Define Safety Factors Based on Integral Experiments," *Proc. Int. Conf. Nuclear Data for Science and Technology*, Gatlinburg, Tennessee, May 9–13, 1994.

37. Y. OYAMA, K. KOSAKO, C. KONNO, Y. IKEDA, F. MAEKAWA, and H. MAEKAWA, "Influence of Selection of Calculation Parameters in Discrete Ordinate Code DOT3.5 for Analysis of Fusion Blanket Integral Experiments in JAERI/USDOE Collaborative Program," *Fusion Eng. Des.*, **28**, 636 (1995).

38. P. G. YOUNG, "Evaluation of n+^{7}Li Reactions Using Variance-Covariance Techniques," *Trans. Am Nucl. Soc.*, **39**, 272 (1980).

39. H. MAEKAWA, T. NAKAMURA, S. AZAM, and P.-A. HALDY, "International Comparison on Measuring Techniques of Tritium Production Rate for Fusion Neutronics Experiments," Interim NEACRP Report NEACRP-A-1021, Nuclear Energy Agency Committee on Reactor Physics (1989); see also *Proc. Annual USDOE/JAERI Workshop on Fusion Blanket Neutronics and the Informal Int. Mtg. Fusion Neutronics*, UCLA-FNT-60, ENG-93-15, University of California, Los Angeles (Aug. 1992).

Mahmoud Z. Youssef (PhD, nuclear engineering, University of Wisconsin, 1980) is a senior research engineer in the Department of Mechanical, Aerospace, and Nuclear Engineering at the University of California, Los Angeles (UCLA). He participated in several conceptual magnetic fusion energy (MFE) and inertial fusion energy (IFE) reactor design studies with emphasis on nuclear analysis and blanket/shield design. His research interests are in the areas of blanket/shield design optimization, nuclear data, sensitivity/uncertainty studies, neutronics methods and code development, tritium fuel cycle, radioactivity and safety aspects of fusion, integral experiments, neutronics testing, and research and development (R&D) for fusion reactors, particularly the International Thermonuclear Experimental Reactor (ITER).

Anil Kumar (PhD, University of Bombay, India, 1981) is senior development engineer at UCLA. His current research interests include fusion reactor nucleonics experiments and analysis, technique development for nuclear heating, decay heat measurements, biological dose, fusion diagnostics, safety factor methodology for fusion reactor design parameters, low-activation materials, inertial confinement fusion, and sequential reactions. He has conducted experiments at leading facilities such as the Fusion Neutronics Source (FNS) facility in Japan, the Tokamak Fusion Test Reactor (TFTR) at Princeton University, and LOTUS in Switzerland.

Mohamed A. Abdou is a professor in the Department of Mechanical, Aerospace, and Nuclear Engineering at UCLA and also is the director of fusion technology at UCLA. His research interests include neutronics, thermomechanics, fusion technology, and reactor design and analysis. He served as the U.S. leader of the Japan Atomic Energy Research Institute (JAERI)/U.S. Department of Energy (U.S. DOE) collaboration on fusion blanket neutronics.

Yoichi Watanabe (PhD, nuclear engineering, University of Wisconsin–Madison) is currently a research fellow at Memorial Sloan-Kettering Cancer Center in New York City and specializes in radiation physics and radiotherapy physics. He has done research in fusion engineering, space nuclear power engineering, and nuclear plasma physics.

Masayuki Nakagawa (BS, 1965; MS, 1967; and PhD, 1979, nuclear engineering, Kyoto University, Japan) is a principal scientist in the Department of Reactor Engineering at JAERI. He is a head of the reactor system laboratory having the main responsibility for the computation method and design of reactors. He researched the development of neutronics computation methods and codes for fast reactors and fusion reactors and intelligent reactor design systems. His group has developed high-speed general-purpose Monte Carlo codes based on vector and/or parallel algorithms.

Kazuaki Kosako (BE, atomic engineering, Tokai University, Japan, 1984) has worked at Sumitomo Atomic Energy Industries since 1994. He worked in the Department of Reactor Engineering at JAERI from 1984 to 1992 where he was involved mainly in fusion neutronics. He is currently interested in the area of radiation damage of materials.

Takamasa Mori (BS, 1976; MS, 1979; and PhD, 1985, nuclear engineering, Kyoto University, Japan) is a principal scientist in the Department of Reactor Engineering at JAERI. He worked for the development of neutron transport codes using double-differential form cross sections. His research interests are in the field of reactor physics, especially the speedup of Monte Carlo calculation of high-energy particles based on vector and/or parallel algorithms.

Yukio Oyama (BS, physics, 1975; MS, nuclear physics, 1977; and Dr. Eng., 1989, Osaka University, Japan) is a principal scientist at JAERI. He has worked in the area of fusion neutronics experiments since 1978. He is currently involved in intense and high-energy neutron source projects.

Chikara Konno (MS, physics, Kyoto University, Japan, 1985) is a research scientist in the Department of Reactor Engineering at JAERI. He has worked in the areas of fusion neutronics experiments, cross-section measurements, and neutron spectrum measurements using a proton-recoil counter.

Yujiro Ikeda (PhD, nuclear engineering, Nagoya University, Japan, 1981) is head of the Fusion Neutronics Laboratory in the Department of Reactor Engineering at JAERI. He has worked in the areas of fusion neutronics experiments, induced radioactivity experiment and analysis, direct nuclear heating measurements, activation cross-section measurements, and fusion dosimetry.

Hiroshi Maekawa (BE, 1965; MS, 1967; and Dr. Eng., 1970, nuclear engineering, Tokyo Institute of Technology, Japan) is the deputy director of the Department of Reactor Engineering and the head of the Intense Neutron Source Laboratory at JAERI. He has worked on fusion neutronics for more than 20 years, and he planned and constructed the FNS facility. He served as the Japanese leader of the JAERI/U.S. DOE collaboration on fusion blanket neutronics. His recent research has focused on International Fusion Materials Irradiation Facility conceptual design activities.

Tomoo Nakamura (BS, physics, Kyoto University, Japan, 1957) is currently director of the Public Acceptance Database Center, Research Organization for Information Science and Technology. His research background includes experimental reactor physics on fast breeder reactors and nuclear technology on fusion reactor blankets. He served as the former Japanese leader of the JAERI/U.S. DOE collaboration on fusion blanket neutronics.